CD59, CD73, CD 90, CD105 and CD166, and negative for CD14, CD31, CD34 and CD45.

Next we investigated whether chorionic plate cells have cardiomyogenic potential by human cardiomyocyte-specific gene expression using RT-PCR method (Fig. 2, Table 1) and gene chip analysis (Table 2; GEO accession number, GSE7021: GSM162104 and GSM162105). Chorionic plate cells expressed Csx/Nkx-2.5, GATA4, BNP, cardiac troponin T (cTnT), cardiac

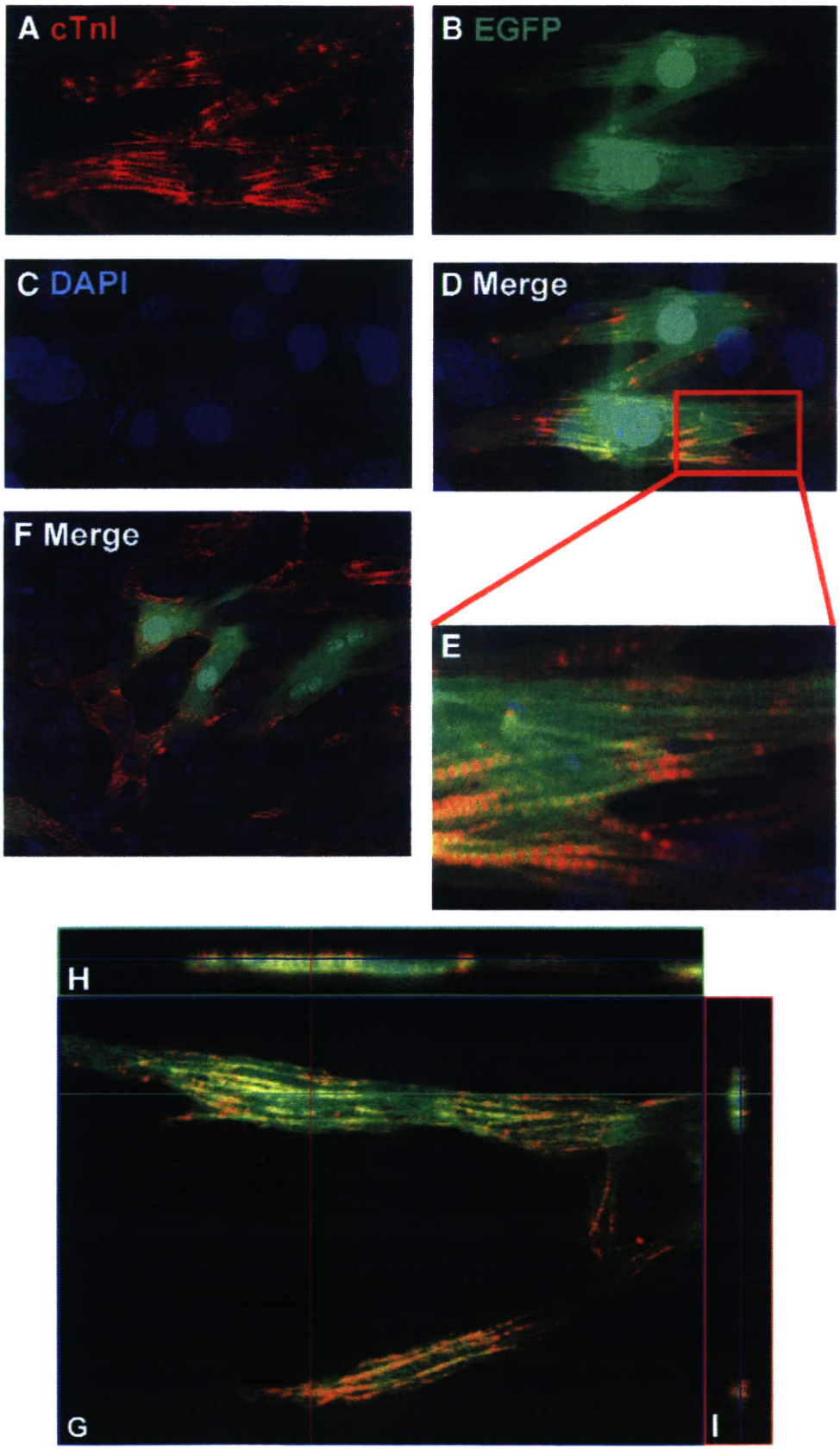

actin and myosin light chain-2α (MLC-2α) in the default state, implying that chorionic plate cells can differentiate into cardiomyocytes, like CMG cells in which Csx/Nkx-2.5 and GATA4 are constitutively expressed before induction [12].

Cardiomyogenic differentiation of chorionic plate cells

employed a co-culture system with murine fetal cardiomyocytes to induce cardiac differentiation, since in vitro simulation of the heart by the environment has been shown to be an efficient means of inducing the differentiation of human endothelial progenitor cells [15] and human marrow stromal cells [13]. EGFP-labeled chorionic plate cells were co-cultured with murine fetal cardiomyocytes without any chemical treatment. A few EGFP-positive chorionic plate cells started to contract on day 3 after the start of co-cultivation, and beat strongly and rigorously in a synchronized manner on day 5 (Supplementary movie 1). The cells continued to beat at least until day 21 during the period of observation. The frequency of cardiomyogenic differentiation from chorionic plate cells was calculated based on the number of cTnI-positive cells. In three independent experiments, the percentage of cells that underwent cardiomyogenic differentiation was similar (15.1±5.1%) (Supplementary Fig. 1S). Our investigation of the cardiomyogenic-specific gene expression for differentiated chorionic plate cells (Fig. 2) found that cardiac actin was fully expressed, whereas Csx/Nkx-2.5 and cardiac troponin T were only slightly expressed. GATA4, cTnI, MLC-2α, and BNP were not expressed. Technical difficulties may have adversely affected these results, as some of the differentiated cells divided from murine fetal cardiomyocytes were physically damaged and so the ratio of differentiated to undifferentiated cells may well have been diminished in each case. In fact, in every experiment, cTnI was detected by immunocytochemical analysis. Immunocytochemical staining revealed that EGFP-labeled cells stained positive for cTnI (Figs. 3A–F). Immunostaining of longitudinal sagittal and axial transverse sections confirmed that cTnI was expressed in the EGFP-positive cells (Figs. 3G–I, Supplementary movie 2). These results imply that co-culture system of chorionic plate cells and murine embryonic cardiomyocytes induces differentiation of chorionic plate cells into cTnI-positive cells in vitro. cTnI-positive cells were evenly detected throughout the dish, suggesting that the cardiomyogenic induction rate was quite high in the present model. The EGFP-positive cells also expressed α-actinin, and connexin 43 (Figs. 4A–E). Clear striations were observed for the red fluorescence of cTnI (Fig. 3A) and α-actinin (Fig. 4A) in the differentiated chorionic plate cells. Connexin 43 staining (Figs. 4C–G) showed a clear and diffuse pattern around the margin of the cytoplasm, suggesting that these human transdifferentiated cardiomyocytes have tight electrical coupling with each other. We also performed in vivo implantation of EGFP-labeled chorionic plate donor cells into the ischemic heart model of nude rats (data not shown). EGFP-labeled chorionic plate donor cells exhibit positive cTnI reactivities at the implanted site. However, the frequency of cTnI-positive cells in vivo is not comparative with that in vitro.

To investigate if chorionic plate cells are capable of differentiating into osteoblasts and adipocytes [19,20], we induced chorionic to differentiate into osteocytes and adipocytes under specific culture conditions. Chorionic plate cells did not show clear adipogenic and osteogenic differentiation: cells did not accumulate Oil Red O-positive fat droplets and calcium, and did not increase alkaline phosphatase osteogenic activity (Supplementary Fig. 2S), suggesting that chorionic plate cells have a cardiomyocyte potential, but not adipocyte or osteoblast potential.

The action potential of differentiated chorionic plate cells

To detect the electrophysiological coupling due to gap-junctional communication between beating cardiomyocytes, action potentials (APs) were recorded from spontaneously beating EGFP-positive cells. Alexa568 was injected into cells via a recording microelectrode to stain the cells and to confirm that the APs were generated by EGFP-positive cells (Figs. 5A–C). The dye did not diffuse into the murine cardiomyocytes, indicating that there were no tight cell-to-cell heterologous connections, i.e., gap junctions. Alexa568 dye did not diffuse into adjacent human and murine cells of the injected cells that exhibited action potentials. The action potentials obtained originate from human chorionic plate cells or may result from electrical coupling with adjacent cardiomyocytes [24]. The APs obtained from chorionic plate cells showed clear cardiomyocyte-specific sustained plateaux (Figs. 5D, E) and were therefore concluded to be APs of cardiomyocytes, not of smooth muscle cells, nerve cells, or skeletal muscle cells. The measured parameters of the recorded AP were averaged (Fig. 5F). Chorionic plate cells had the character of 'working' cardiomyocytes or ordinary cardiomyocytes. The rhythm of almost all the beating cells had become regular at 1 week. The fractional shortening (%FS) of the cells was analyzed (Supplementary Fig. 3S), using a cell-edge detection program developed by S.M. The EGFP-positive cells contracted simultaneously within the whole visual field, suggesting tight electrical communication among them. The average %FS was 5.46±0.40% ($n=10$). In summary, human cardiomyocytes obtained from the chorionic plate cells were electrophysiologically and physiologically functional.

Discussion

Transdifferentiation of human extraembryonic mesodermal cells into embryonic mesodermal cells: functional working cardiomyocytes

This study was conducted to determine whether extensive ex vivo propagation by cell culture would prevent the cardiomyogenic differentiation of placenta-derived cells. According to our previous study on the induction of cardiomyogenic differentiation of immortalized murine marrow stromal cells [12,15] and human marrow stromal cells [13] by demethylating agents, the transdifferentiation of human stromal cells was limited to working cardiomyocytes and did not include pacemaker cells. This was probably due to the origin of cells, that is, the default state of the chorionic plate-derived human fetal cells used in the experiment. The idea for the cardiomyogenic differentiation protocol using murine fetal cardiomyocytes without 5-azacytidine arose from reports that endothelial cells differentiate into cardiomyocytes as a result of co-cultivation with murine fetal cardiomyocytes [25].

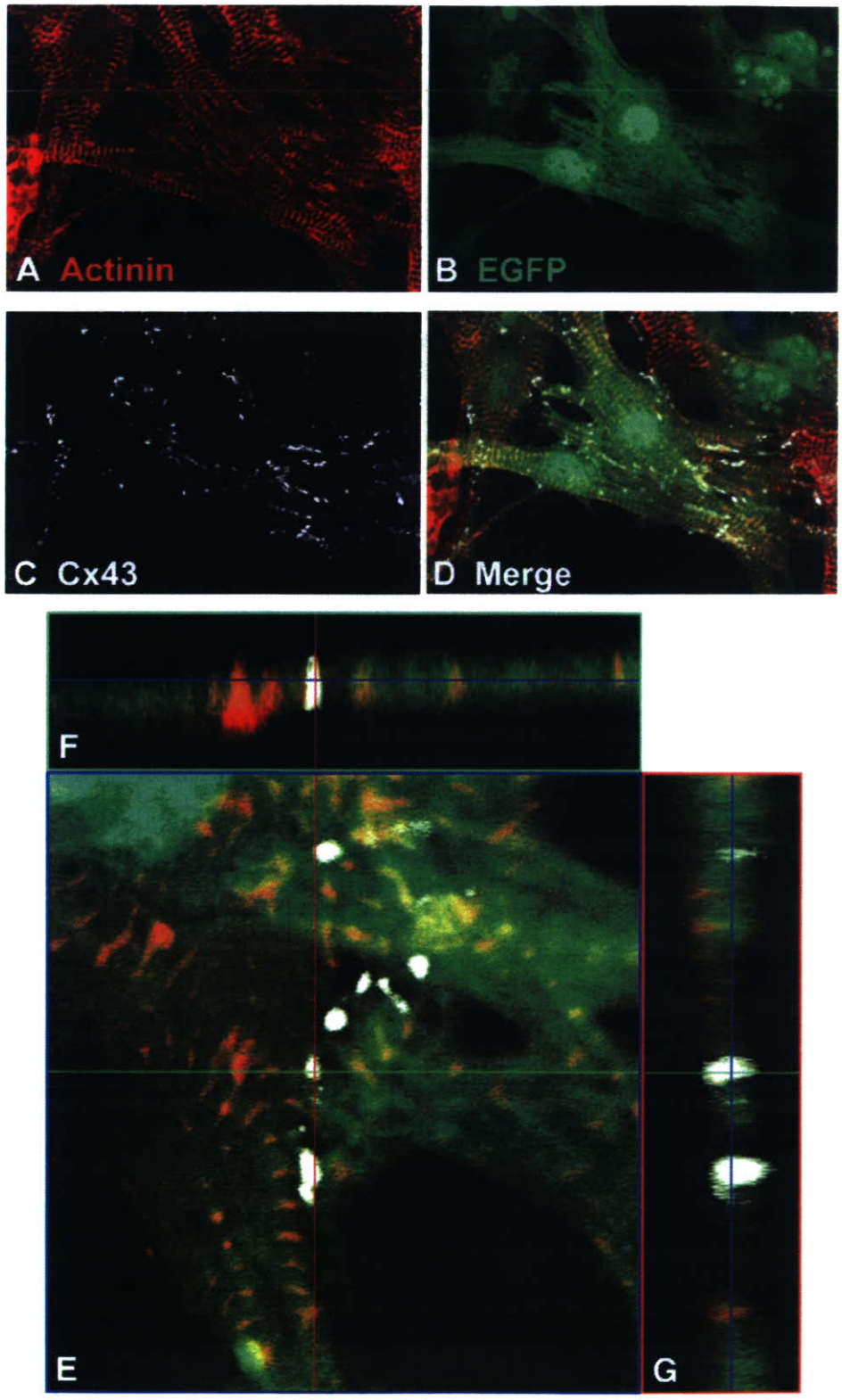

Fig. 4 – Immunocytochemistry of chorionic plate cells for α-actinin and connexin 43. (A–D) Immunocytochemistry of differentiated chorionic plate cells for α-actinin (Actinin) and connexin 43 (Cx43) antibody. Clear striations were observed for the red fluorescence of α-actinin (A) in the EGFP-positive cells (B). Connexin 43 (C) was stained along the attachment site of EGFP-positive cells. Merged images (α-actinin, connexin 43, EGFP) are shown in panel D. (E–G) A merged image for α-actinin, connexin 43, and EGFP is shown in panel E. (F) A longitudinal section at the green line in merged image E. (G) An axial section at the red line in merged image E. Panels F and G show that connexin 43 is located between EGFP-positive cells.

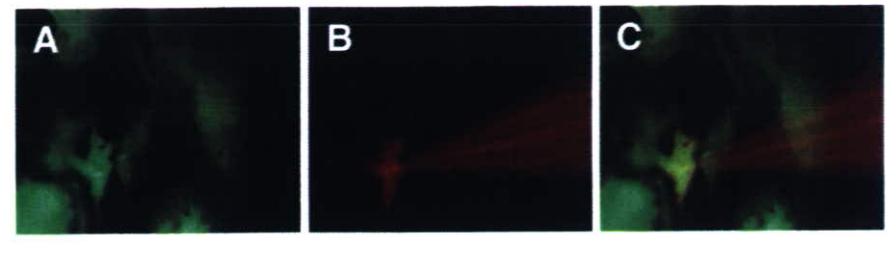

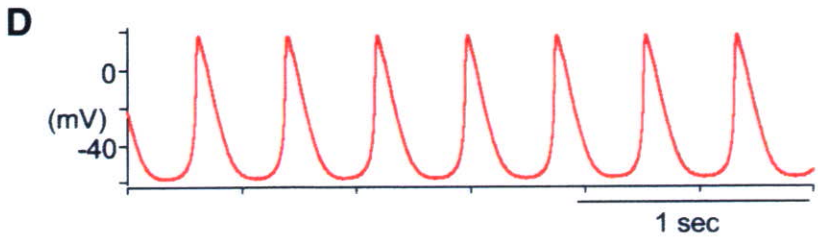

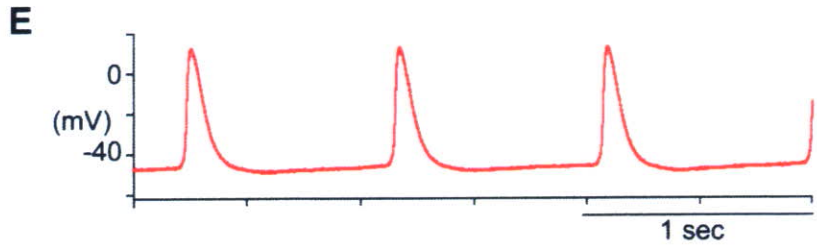

F

	Amplitude (mV)	Resting Membrane Potential (mV)	APD90 (msec)	APD50 (msec)	RR (sec)	Vmax (V/s)	n
PLKC	63.87± 2.24	-52.22± 1.05	209.1± 12.9	100.2± 4.8	0.948± 0.138	4.460± 0.355	14

Fig. 5 – Electrophysiological and physiological analysis of chorionic plate cells. (A–C) EGFP-labeled chorionic plate cells were injected with Alexa568 solution by ionophoresis through a microelectrode. (D, E) Two different types of action potential, i.e., tachycardia type and bradycardia type, were recorded. Both types of cells had the features of working cardiomyocytes. The rhythm of their beating was regular. (F) The measured action potential parameters of EGFP-labeled chorionic plate cells are averaged.

The high frequency of cardiomyogenic differentiation makes it inconceivable that the transdifferentiation is due to fusion; in addition, bone marrow stromal cells [13] do not fuse with feeder cells in the co-cultivation system and the frequency of fusion in the co-culture system is not high [26] in contrast to myogenic differentiation [27]. The global gene expression pattern showed that the change in gene expression during differentiation was consistent with phenotypic alteration. The cells established from the placenta can be extensively and clonally expanded in vitro while retaining their potential to differentiate into cardiomyocytes that exhibit spontaneous beating and cardiomyocyte-specific action potential under in vitro conditions. This differentiation potential shown by the placenta-derived cells is the same as that reported for bone marrow MSCs [12,13,15]. It is also noteworthy that the transdifferentiation of chorionic plate cells represents the transition from extraembryonic cells to embryonic cells, while the transdifferentiation from bone-marrow-derived MSCs to neurogenic cells, which we previously reported [28,29], is transition between germ layers in embryonic tissues.

Most of the surface markers of the placenta-derived cells examined in this study are the same as those detected in their bone marrow counterparts [13,30], with both cord blood- and bone-marrow-derived mesodermal cells being positive for CD29, CD44, and CD59, and negative for CD34. Our finding of in vitro differentiation from extraembryonic mesodermal cells to embryonic mesodermal cells in this study, a key future goal for any cell-based therapy, could thus be achieved by exposing placenta-derived cells to murine fetal cardiomyocytes, at least in vitro. This technique allows the applications of the placenta to be further extended and permits it to be used as an alternative to bone marrow as a source of cells with cardiomyogenic potential.

Is the high rate of cardiomyogenic differentiation of placenta-derived cells due to the default cell state?

The cardiomyogenic differentiation rate of chorionic plate cells (15.1%) was relatively high compared to that of marrow-derived MSCs (less than 0.3%) [13]. The gene expression

pattern of chorionic plate cells before cardiomyogenic differentiation was different from that of marrow-derived MSCs. The expression of cardiomyocyte-associated genes in the chorionic plate cells, which we unexpectedly found by GeneChip analysis and confirmed by RT-PCR, is surprising. Constitutive expression of the Csx/Nkx2.5 cardiogenic 'master' gene [31,32] in the chorionic plate cells with the ability of self-renewal suggests that the chorionic plate cells have cardiogenic potential [33] and may be termed "cardiac precursor cells" in the light of their biological characteristics like endometrium-derived myogenic procursor cells [27]. The mechanism of the drastic improvement in the differentiation rate of chorionic plate cells may be attributable to default characteristics as cardiac precursor cells of the placenta-derived cells in culture. Because of this improvement in the differentiation rate, it is possible to obtain a large number of cardiomyocytes without prolongation of their life span, i.e., transfer of oncogenic molecules into cells, to restore cardiac function. It is quite interesting that working cardiomyocytes can be generated from placenta-derived cells, since one of the types of target cells for regenerative medicine is heart cells.

Are human placenta-derived cells that are propagated in vitro useful for cell-based therapy?

Can primary placenta-derived cell 'culture' contribute to cell-based therapy or regenerative medicine? Primary placenta-derived cell culture obtained from the chorionic mesodermal layer succeeded in almost 100% of the attempts, and the cells were passaged only 3 or 4 times (6 to 7 PDs) before reaching premature senescence. The problems involved in cell-based therapy with human placenta-derived cells are the finite life span of the cells and the difficulty of obtaining a large enough number of cells. Based on the results of our previous study using cord blood-derived cells, the establishment of cells can be explained by: (1), lack of $p16^{INK4a}$ in primary-cultured cells, or (2), selection of cells that do not express $p16^{INK4a}$ from a heterogeneous population [22]. We cannot exclude either possibility, and we did observe two different types of cells, i.e., rapidly growing spindle cells and quiescent flat and elongated cells in the primary culture of placenta cells. Experimental settings that allow human placenta cells to double more than 100 times may be used to obtain a large number of cells at least from the placenta.

We believe that these placenta-derived extraembryonic mesodermal cells may be used to supply cardiomyocytes to patients with ischemic heart disease, dilated cardiomyopathy, and Kawasaki disease, which all have a poor prognosis and are sometimes lethal. The 'risk versus benefit' balance is essential when applying these multiplied cells clinically and the 'risk' or 'drawback' in this case is the transformation of implanted cells. In vivo experiments revealed that no tumor was observed for up to 4 weeks when chorionic plate cells at P5 (1×10^7) were subcutaneously inoculated into immunodeficient, non-obese diabetic (NOD)/severe combined immunodeficiency (SCID)/interleukin 2 $receptor^{-/-}$ (NOG) mice (data not shown). Human placenta-derived cells spontaneously avoid premature senescence without gene induction and enter replicative senescence. Replicative senescence may be due to a tumor suppressor mechanism that avoids the risk of cell transformation after implantation of cells as a source for cell-based therapy [34].

Our present study suggested the presence of a precursor cell type in the placenta which is destined to generate 'working cardiomyocytes'. Since the placenta is usually discarded, it can be collected at usual delivery or cesarean section and can be banked or stored. Cells with almost all the HLA types can be collected after several generations. A placenta-derived cell bank system covering all HLA types may be necessary for patients who cannot supply bone marrow cells but want to receive stem cell-based cardiac therapy.

Acknowledgments

We would like to express our sincere thanks to A. Crump for critically reading the manuscript, A. Oka and M. Terai for the support throughout the work, and K. Saito for the secretarial work. This study was supported by grants from the Ministry of Education, Culture, Sports, Science and Technology (MEXT) of Japan; by the Suntory Fund for Advanced Cardiac Therapeutics, Keio University School of Medicine; Health and Labor Sciences Research Grants, and the Pharmaceuticals and Medical Devices Agency; by the Research on Health Science Focusing on Drug Innovation from the Japan Health Science Foundation; by the Program for Promotion of Fundamental Studies in Health Science of the Pharmaceuticals and Medical Devices Agency (PMDA); by a research Grant for Cardiovascular Disease from the Ministry of Health, Labor and Welfare; by a Grant for Child Health and Development from the Ministry of Health, Labor and Welfare; and by a grant from Terumo Life Science Foundation. A part of the work was done at the Pfizer Keio Research Laboratory Center for Integrated Medical Research.

Data set from the gene chip analysis are available at the GEO database with accession number GSE7021: GSM162104 and GSM162105.

Appendix A. Supplementary data

Supplementary data associated with this article can be found, in the online version, at doi:10.1016/j.yexcr.2007.04.028.

REFERENCES

[1] T. Thom, N. Haase, W. Rosamond, V.J. Howard, J. Rumsfeld, T. Manolio, Z.J. Zheng, K. Flegal, C. O'Donnell, S. Kittner, D. Lloyd-Jones, D.C. Goff Jr., Y. Hong, R. Adams, G. Friday, K. Furie, P. Gorelick, B. Kissela, J. Marler, J. Meigs, V. Roger, S. Sidney, P. Sorlie, J. Steinberger, S. Wasserthiel-Smoller, M. Wilson, P. Wolf, Heart disease and stroke statistics—2006 update: a report from the American Heart Association Statistics Committee and Stroke Statistics Subcommittee, Circulation 113 (2006) e85–e151.

[2] A. Leri, J. Kajstura, P. Anversa, Cardiac stem cells and mechanisms of myocardial regeneration, Physiol. Rev. 85 (2005) 1373–1416.

[3] M.A. Laflamme, C.E. Murry, Regenerating the heart, Nat. Biotechnol. 23 (2005) 845–856.

[4] H.F. Tse, Y.L. Kwong, J.K. Chan, G. Lo, C.L. Ho, C.P. Lau, Angiogenesis in ischaemic myocardium by intramyocardial autologous bone marrow mononuclear cell implantation, Lancet 361 (2003) 47–49.
[5] E. Perin, Transendocardial injection of autologous mononuclear bone marrow cells in end-stage ischemic heart failure patients: one-year follow-up, Int. J. Cardiol. 95 (Suppl 1) (2004) S45–S46.
[6] K.C. Wollert, G.P. Meyer, J. Lotz, S. Ringes-Lichtenberg, P. Lippolt, C. Breidenbach, S. Fichtner, T. Korte, B. Hornig, D. Messinger, L. Arseniev, B. Hertenstein, A. Ganser, H. Drexler, Intracoronary autologous bone-marrow cell transfer after myocardial infarction: the BOOST randomised controlled clinical trial, Lancet 364 (2004) 141–148.
[7] O. Agbulut, S. Vandervelde, N. Al Attar, J. Larghero, S. Ghostine, B. Leobon, E. Robidel, P. Borsani, M. Le Lorc'h, A. Bissery, C. Chomienne, P. Bruneval, J.P. Marolleau, J.T. Vilquin, A. Hagege, J.L. Samuel, P. Menasche, Comparison of human skeletal myoblasts and bone marrow-derived CD133+ progenitors for the repair of infarcted myocardium, J. Am. Coll. Cardiol. 44 (2004) 458–463.
[8] P. Menasche, A.A. Hagege, M. Scorsin, B. Pouzet, M. Desnos, D. Duboc, K. Schwartz, J.T. Vilquin, J.P. Marolleau, Myoblast transplantation for heart failure, Lancet 357 (2001) 279–280.
[9] D.J. Prockop, Stem cell research has only just begun, Science 293 (2001) 211–212.
[10] K. Le Blanc, C. Gotherstrom, O. Ringden, M. Hassan, R. McMahon, E. Horwitz, G. Anneren, O. Axelsson, J. Nunn, U. Ewald, S. Norden-Lindeberg, M. Jansson, A. Dalton, E. Astrom, M. Westgren, Fetal mesenchymal stem-cell engraftment in bone after in utero transplantation in a patient with severe osteogenesis imperfecta, Transplantation 79 (2005) 1607–1614.
[11] K. Le Blanc, I. Rasmusson, C. Gotherstrom, C. Seidel, B. Sundberg, M. Sundin, K. Rosendahl, C. Tammik, O. Ringden, Mesenchymal stem cells inhibit the expression of CD25 (interleukin-2 receptor) and CD38 on phytohaemagglutinin-activated lymphocytes, Scand. J. Immunol. 60 (2004) 307–315.
[12] S. Makino, K. Fukuda, S. Miyoshi, F. Konishi, H. Kodama, J. Pan, M. Sano, T. Takahashi, S. Hori, H. Abe, J. Hata, A. Umezawa, S. Ogawa, Cardiomyocytes can be generated from marrow stromal cells in vitro, J. Clin. Invest. 103 (1999) 697–705.
[13] Y. Takeda, T. Mori, H. Imabayashi, T. Kiyono, S. Gojo, S. Miyoshi, N. Hida, M. Ita, K. Segawa, S. Ogawa, M. Sakamoto, S. Nakamura, A. Umezawa, Can the life span of human marrow stromal cells be prolonged by bmi-1, E6, E7, and/or telomerase without affecting cardiomyogenic differentiation? J. Gene Med. 6 (2004) 833–845.
[14] D. Orlic, J. Kajstura, S. Chimenti, I. Jakoniuk, S.M. Anderson, B. Li, J. Pickel, R. McKay, B. Nadal-Ginard, D.M. Bodine, A. Leri, P. Anversa, Bone marrow cells regenerate infarcted myocardium, Nature 410 (2001) 701–705.
[15] S. Gojo, N. Gojo, Y. Takeda, T. Mori, H. Abe, S. Kyo, J. Hata, A. Umezawa, In vivo cardiovasculogenesis by direct injection of isolated adult mesenchymal stem cells, Exp. Cell Res. 288 (2003) 51–59.
[16] J.S. Wang, D. Shum-Tim, J. Galipeau, E. Chedrawy, N. Eliopoulos, R.C. Chiu, Marrow stromal cells for cellular cardiomyoplasty: feasibility and potential clinical advantages, J. Thorac. Cardiovasc. Surg. 120 (2000) 999–1005.
[17] J.G. Shake, P.J. Gruber, W.A. Baumgartner, G. Senechal, J. Meyers, J.M. Redmond, M.F. Pittenger, B.J. Martin, Mesenchymal stem cell implantation in a swine myocardial infarct model: engraftment and functional effects, Ann. Thorac. Surg. 73 (2002) 1919–1925 (discussion 1926).
[18] K.L. Moore, T.V.N. Persaud, The Developing Human: Clinically Oriented Embryology, Saunders, Philadelphia, Pa., 2003.
[19] K. Igura, X. Zhang, K. Takahashi, A. Mitsuru, S. Yamaguchi, T.A. Takashi, Isolation and characterization of mesenchymal progenitor cells from chorionic villi of human placenta, Cytotherapy 6 (2004) 543–553.
[20] X. Zhang, A. Mitsuru, K. Igura, K. Takahashi, S. Ichinose, S. Yamaguchi, T.A. Takahashi, Mesenchymal progenitor cells derived from chorionic villi of human placenta for cartilage tissue engineering, Biochem. Biophys. Res. Commun. 340 (2006) 944–952.
[21] J. Paquin, B.A. Danalache, M. Jankowski, S.M. McCann, J. Gutkowska, Oxytocin induces differentiation of P19 embryonic stem cells to cardiomyocytes, Proc. Natl. Acad. Sci. U. S. A. 99 (2002) 9550–9555.
[22] M. Terai, T. Uyama, T. Sugiki, X.K. Li, A. Umezawa, T. Kiyono, Immortalization of human fetal cells: the life span of umbilical cord blood-derived cells can be prolonged without manipulating p16INK4a/RB braking pathway, Mol. Biol. Cell 16 (2005) 1491–1499.
[23] D.J. Prockop, I. Sekiya, D.C. Colter, Isolation and characterization of rapidly self-renewing stem cells from cultures of human marrow stromal cells, Cytotherapy 3 (2001) 393–396.
[24] I. Potapova, A. Plotnikov, Z. Lu, P. Danilo Jr., V. Valiunas, J. Qu, S. Doronin, J. Zuckerman, I.N. Shlapakova, J. Gao, Z. Pan, A.J. Herron, R.B. Robinson, P.R. Brink, M.R. Rosen, I.S. Cohen, Human mesenchymal stem cells as a gene delivery system to create cardiac pacemakers, Circ. Res. 94 (2004) 952–959.
[25] C. Badorff, R.P. Brandes, R. Popp, S. Rupp, C. Urbich, A. Aicher, I. Fleming, R. Busse, A.M. Zeiher, S. Dimmeler, Transdifferentiation of blood-derived human adult endothelial progenitor cells into functionally active cardiomyocytes, Circulation 107 (2003) 1024–1032.
[26] K. Matsuura, H. Wada, T. Nagai, Y. Iijima, T. Minamino, M. Sano, H. Akazawa, J.D. Molkentin, H. Kasanuki, I. Komuro, Cardiomyocytes fuse with surrounding noncardiomyocytes and reenter the cell cycle, J. Cell Biol. 167 (2004) 351–363.
[27] C.H. Cui, T. Uyama, K. Miyado, M. Terai, S. Kyo, T. Kiyono, A. Umezawa, Menstrual blood-derived cells confer human dystrophin expression in the murine model of duchenne muscular dystrophy via cell fusion and myogenic transdifferentiation, Mol. Biol. Cell 18 (2007) 1586–1594.
[28] T. Mori, T. Kiyono, H. Imabayashi, Y. Takeda, K. Tsuchiya, S. Miyoshi, H. Makino, K. Matsumoto, H. Saito, S. Ogawa, M. Sakamoto, J. Hata, A. Umezawa, Combination of hTERT and bmi-1, E6, or E7 induces prolongation of the life span of bone marrow stromal cells from an elderly donor without affecting their neurogenic potential, Mol. Cell. Biol. 25 (2005) 5183–5195.
[29] J. Kohyama, H. Abe, T. Shimazaki, A. Koizumi, K. Nakashima, S. Gojo, T. Taga, H. Okano, J. Hata, A. Umezawa, Brain from bone: efficient "meta-differentiation" of marrow stroma-derived mature osteoblasts to neurons with Noggin or a demethylating agent, Differentiation 68 (2001) 235–244.
[30] K.D. Lee, T.K. Kuo, J. Whang-Peng, Y.F. Chung, C.T. Lin, S.H. Chou, J.R. Chen, Y.P. Chen, O.K. Lee, In vitro hepatic differentiation of human mesenchymal stem cells Hepatology 40 (2004) 1275–1284.
[31] I. Komuro, S. Izumo, Csx: a murine homeobox-containing gene specifically expressed in the developing heart, Proc. Natl. Acad. Sci. U. S. A. 90 (1993) 8145–8149.
[32] I. Shiojima, I. Komuro, T. Mizuno, R. Aikawa, H. Akazawa, T. Oka, T. Yamazaki, Y. Yazaki, Molecular cloning and characterization of human cardiac homeobox gene CSX1, Circ. Res. 79 (1996) 920–929.
[33] Y. Yamada, K. Sakurada, Y. Takeda, S. Gojo, A. Umezawa, Single-cell-derived mesenchymal stem cells overexpressing Csx/Nkx2.5 and GATA4 undergo the stochastic cardiomyogenic fate and behave like transient amplifying cells, Exp. Cell Res. 313 (2007) 698–706.
[34] F. Ishikawa, Cellular senescence, an unpopular yet trustworthy tumor suppressor mechanism, Cancer Sci. 94 (2003) 944–947.

STEM CELLS

TISSUE-SPECIFIC STEM CELLS

Administration of Granulocyte Colony-Stimulating Factor After Myocardial Infarction Enhances the Recruitment of Hematopoietic Stem Cell-Derived Myofibroblasts and Contributes to Cardiac Repair

JUN FUJITA,[a] MITSUHARU MORI,[c] HIROSHI KAWADA,[e,f] YASUYO IEDA,[a] MITSUYO TSUMA,[e,f] YUMI MATSUZAKI,[d] HARUKO KAWAGUCHI,[a] TAKASHI YAGI,[a] SHINSUKE YUASA,[a] JIN ENDO,[a] TOMOMITSU HOTTA,[e,f] SATOSHI OGAWA,[b] HIDEYUKI OKANO,[d] RYOHEI YOZU,[c] KIYOSHI ANDO,[e,f] KEIICHI FUKUDA[a]

[a]Department of Regenerative Medicine and Advanced Cardiac Therapeutics, [b]Division of Cardiology, Department of Internal Medicine, [c]Department of Cardiac Surgery, and [d]Department of Physiology, Keio University School of Medicine, Shinjuku-ku, Tokyo, Japan; [e]Department of Medicine and [f]Research Center for Regenerative Medicine, Tokai University School of Medicine, Isehara, Kanagawa, Japan

Key Words. Myofibroblasts/fibroblasts • Monocytes/macrophages • Hematopoietic stem cells • Myocardial infarction Granulocyte colony-stimulating factor

ABSTRACT

The administration of granulocyte colony-stimulating factor (G-CSF) after myocardial infarction (MI) improves cardiac function and survival rates in mice. It was also reported recently that bone marrow (BM)-derived c-kit$^+$ cells or macrophages in the infarcted heart are associated with improvement of cardiac remodeling and function. These observations prompted us to examine whether BM-derived hematopoietic cells mobilized by G-CSF administration after MI play a beneficial role in the infarct region. A single hematopoietic stem cell from green fluorescent protein (GFP)-transgenic mice was used to reconstitute hematopoiesis in each experimental mouse. MI was then induced, and the mice received G-CSF for 10 days. In the acute phase, a number of GFP$^+$ cells showing the elongated morphology were found in the infarcted area. Most of these cells were positive for vimentin and α-smooth muscle actin but negative for CD45, indicating that they were myofibroblasts. The number of these cells was markedly enhanced by G-CSF administration, and the enhanced myofibroblast-rich repair was considered to lead to improvements of cardiac remodeling, function, and survival rate. Next, G-CSF-mobilized monocytes were harvested from the peripheral blood of GFP-transgenic mice and injected intravenously into the infarcted mice. Following this procedure, GFP$^+$ myofibroblasts were observed in the infarcted myocardium. These results indicate that cardiac myofibroblasts are hematopoietic in origin and could arise from monocytes/macrophages. MI leads to the recruitment of monocytes, which differentiate into myofibroblasts in the infarct region. Administration of G-CSF promotes this recruitment and enhances cardiac protection. STEM CELLS *2007;25:2750–2759*

Disclosure of potential conflicts of interest is found at the end of this article.

INTRODUCTION

Bone marrow (BM) cells were implicated recently in the repair of heart tissue following myocardial infarction (MI) [1–3]. In addition, the administration of granulocyte colony-stimulating factor (G-CSF) alone or in combination with stem cell factor can improve cardiac function and survival rate in mice, mobilizing BM cells to the infarcted region in the heart [4, 5]. BM contains both hematopoietic stem cells (HSCs) and mesenchymal stem cells (MSCs). Our previous clonal studies in which BM HSCs or MSCs were replaced by green fluorescence protein (GFP)-labeled populations showed, first, that the GFP$^+$ cardiomyocytes were derived primarily from MSCs and, second, that administration of G-CSF improved function and survival preventing cardiac remodeling [6]. However, the number of MSC-derived regenerated cardiomyocytes was considered insufficient to account solely for the beneficial effect of G-CSF on cardiac remodeling.

A very recent study found that MI increased the number of BM-derived cells positive for the HSC marker c-kit in infarcted murine hearts [7]. In addition, the recruitment of BM-derived cells was associated with endothelial mitogenesis and establishment of an extensive myofibroblast-rich repair tissue, resulting in prevention of cardiac failure and death. Leor et al. [8] also reported that injection of ex vivo-activated macrophages derived

Correspondence: Hiroshi Kawada, M.D., Ph.D., Department of Medicine, Tokai University School of Medicine, 143 Shimokasuya, Isehara, Kanagawa 259-1143, Japan. Telephone: 81-463-93-1121; Fax: 81-463-92-4511; e-mail: hkawada@is.icc.u-tokai.ac.jp; Keiichi Fukuda, Department of Regenerative Medicine and Advanced Cardiac Therapeutics, Keio University School of Medicine, 35 Shinanomachi, Shinjuku-ku, Tokyo 160-8582, Japan. Telephone: 81-3-5363-3874; Fax: 81-3-5363-3875; e-mail: kfukuda@sc.itc.keio.ac.jp Received April 14, 2007; accepted for publication July 27, 2007; first published online in STEM CELLS *EXPRESS* August 9, 2007. 1066-5099/2007/$30.00/0 doi: 10.1634/stemcells.2007-0275

from human peripheral blood monocytes into the ischemic murine myocardium increased scar vessel density and promoted myofibroblast accumulation, resulting in improvement of scar thickening, cardiac remodeling, and function. We therefore speculated that BM-derived hematopoietic cells mobilized by G-CSF after MI might also play a beneficial role in cardiac repair.

This study thus assessed the significance of HSC-derived cells for cardiac repair using a clonal experimental system. We demonstrated that cardiac myofibroblasts/fibroblasts may derive from HSCs and that G-CSF treatment markedly increases the number of HSC-derived myofibroblasts/fibroblasts in the infarcted area, resulting in a reinforced infarcted ventricular wall and improved cardiac remodeling, function, and survival.

METHODS

Animals

C57BL/6 mice were purchased from CLEA Japan (Tokyo, http://www.clea-japan.com). GFP-transgenic mice were a gift from Prof. M. Okabe (Osaka University, Suita, Osaka, Japan) [9]. All experimental procedures and protocols were approved by the Animal Care and Use Committees of Keio and Tokai Universities, Japan.

Isolation of HSCs and BM Transplantation

HSCs were isolated using combined $CD34^-c\text{-}kit^+Sca\text{-}1^+lineage^-$ and tip-side population (tip-SP) cells as described previously [10]. Briefly, BM cells suspended at 1×10^6 cells per milliliter in Hanks' balanced salt solution+ (HBSS+) (calcium- and magnesium-free HBSS supplemented with 2% fetal calf serum, 10 mM HEPES, 100 U/ml penicillin, and 100 μg/ml streptomycin) were incubated with 5 mg/ml Hoechst 33342 (Sigma-Aldrich, St. Louis, http://www.sigmaaldrich.com) for 60 minutes at 37°C. After washing, the cells were resuspended in ice-cold HBSS+ at a cell density of 10^7 cells per milliliter and then stained for 30 minutes on ice with various monoclonal antibodies, including biotinylated CD34, allophycocyanin (APC)-conjugated c-kit, phycoerythrin (PE)-conjugated Sca-1, and PE-Cy5-conjugated lineage markers (Gr-1, Mac-1, B220, CD3, and TER119). The biotinylated antibodies were visualized using PharRed (APC-Cy7)-conjugated streptavidin. All of these reagents were purchased from BD Pharmingen (San Diego, http://www.bdbiosciences.com/index_us.shtml). Cell sorting was performed using a triple laser MoFlo (DakoCytomation, Glostrup, Denmark, http://www.dakocytomation.com) using Summit software. Hoechst 33342 was excited at 350 nm, and the fluorescence emission was detected using 405/BP30 and 570/BP20 optical filters against Hoechst blue and Hoechst red, respectively, and a 555-nm long-pass dichroic mirror (Omega Optics Inc., Austin, TX, http://www.omegaoptics.com) to separate the emission wavelengths. Both Hoechst blue and red fluorescence were shown on a linear scale. After collecting 10^5 events, the tip-SP showing the highest dye efflux (or lowest staining) was defined as described previously [10], and additional gates were defined as positive for Sca-1 and c-kit and negative for CD34 and lineage markers according to the isotype control fluorescence intensity. Populations of $CD34^-c\text{-}kit^+Sca\text{-}1^+lineage^-$ tip-SP ($CD34^-KSL$-tip-SP) cells of 99% purity were routinely prepared using this method, and most were considered to be HSCs because 96% of the lethally irradiated mice that received a single $CD34^-KSL$-tip-SP cell showed significant donor cell engraftment over the long term [10]. Single $CD34^-KSL$-tip-SP cells derived from GFP-transgenic mice were sorted directly into separate wells of a 96-well plate containing 100 μl of HBSS+ using a CyClone automated cell deposition unit (DakoCytomation) they were then intravenously injected (one cell per mouse) into the tail vein of 8–10-week-old C57/BL6 mice that had been lethally irradiated with a dose of 10.5 Gy (HSC group). To prevent death soon after transplantation due to insufficient hematopoietic reconstitution by a transplanted single HSC [11], 2×10^5 radioprotective GFP^- whole BM cells from C57/BL6 mice of the same age as recipients were transplanted together with the single HSC. Whole BM cells (5×10^6) were also obtained from GFP-transgenic mice and transplanted intravenously into irradiated mice (whole bone marrow [w-BM] group) as a control. Twenty weeks after transplantation, peripheral blood was collected, erythrocytes were depleted using Ficoll-Paque, and fluorescence-activated cell sorting (FACS) analysis was performed using a FACSCalibur (BD Biosciences, San Jose, CA, http://www.bdbiosciences.com) to confirm the hematopoietic reconstitution by GFP^+ cells.

MI and Mobilization of BM Cells

The recipient mice were intubated and anesthetized with 0.5% isoflurane. MI was generated by ligation of the left anterior descending coronary artery as described previously [6]. After 24 hours, daily subcutaneous injection of recombinant human G-CSF (300 μg/kg) or saline was started.

Echocardiography and Hemodynamic Measurements

Echocardiography was performed using an Image Point 1500 (Philips, Electronics Japan, Tokyo, http://www.medical.philips.com/jp) with a 15-MHz transducer. Mice were anesthetized with ketamine (30 mg/kg) and xylazine (6 mg/kg) to maintain spontaneous breathing. Left ventricular (LV) internal end-systolic diameter (LVESD) and LV end-diastolic diameter (LVEDD) were measured with the use of the leading-edge convention adapted by the American Society of Echocardiography [12]. LV ejection fraction (EF) was calculated as EF (%) = ([EDV − ESV]/EDV) × 100. LV fractional shortening (FS) was also calculated as FS (%) = ([LVEDD − LVESD]/LVEDD) × 100. A 1.4-F microtip pressure transducer (SPR-671; Millar Instruments, Houston, TX, http://www.millarinstruments.com) was cannulated into the right common carotid artery and advanced into the left ventricle for the evaluation of LV end-diastolic pressure (LVEDP) and LV peaked pressure (LVP), +LVdP/dt.

Determination of Infarct Size

For the measurement of infarct size in acute phase, mice were anesthetized with pentobarbital and sacrificed ($n = 5$ in each group) 7 days after myocardial infarction. The hearts were obtained and sectioned along the short axis. Each section was stained with triphenyltetrazolium chloride (TTC). The TTC-unstained and TTC-stained areas were then measured using a planimetry software program (NIH Image) at the base, middle, and apex levels of the left ventricle, and the percentage of TTC-unstained area compared with total area was calculated for all sections and defined as the infarct area [13].

To measure infarct size in the chronic phase, hearts were perfused from the apex with phosphate-buffered saline (PBS), perfusion-fixed with 4% paraformaldehyde/PBS, dissected, immersion-fixed overnight at 4°C, embedded in Tissue-Tek OCT Compound (Sakura Finetech USA Inc., Torrance, CA, http://www.sakuraeu.com), and quickly frozen in liquid nitrogen. Sections were stained with Azan. The outer perimeter of the infarcted area was measured from one edge of the infarcted area to the other by planimetry software. Each section was sliced to 6 mm, and one of five sections was measured. The outer perimeter was determined using the average of 30 sections of the mid-ventricle in each mouse. The thickness of left ventricle was determined from the averages of the left edge, right edge, and middle of the infarcted area. The mean thickness of left ventricle was also determined from the average of 30 sections of the mid-ventricle by planimetry software.

Fluorescence Photography

Cryostat sections (6 μm) were stained overnight at 4°C with specific antibodies. Anti-α-actinin (clone EA-53; Sigma-Aldrich), anti-α-smooth muscle actin (anti-α-SMA) (clone 1A4; Sigma-Aldrich), anti-vimentin (clone GP53; Progen, Heidelberg, Germany, http://www.progen.de), anti-von Willebrand factor (anti-vWF) (clone F8/86; Dako, Glostrup, Denmark, http://www.dako.com), anti-CD45 (clone 30-F11, H130; BD Pharmingen), and Ki-67 (code PRO229; YLEM Roma, Rome, http://www.ylem.it/index.html) were used as primary antibodies. The sections were incubated with secondary

antibodies conjugated with Alexa 488, Alexa 594, Alexa 660 (Molecular Probes Inc., Eugene, OR, http://probes.invitrogen.com), or tetramethylrhodamine isothiocyanate (Sigma-Aldrich). Nuclei were stained with a dimeric cyanine nucleic acid dye, TOTO-3 (Molecular Probes). Slides were observed using a confocal laser-scanning microscope (LSM510 META-spectrometer; Carl Zeiss, Jena, Germany, http://www.zeiss.com), with online spectral fingerprinting. Quantitative measurements for designated antigen-positive cells were based on the count of the number of the antigen-positive cells in 100 sections of the mid-left ventricle level. The GFP signal of cardiac fibroblasts was confirmed by emission fingerprinting, using an LSM 510 META-spectrometer (Carl Zeiss).

Isolation and Transplantation of Murine Monocytes

The murine monocyte fraction was prepared from peripheral blood of GFP-transgenic mice stimulated with G-CSF (300 μg/kg) for 5 days using Nyco Prep (Axis-Shield, Oslo, Norway, http://www.axis-shield-poc.com) according to the manufacturer's instructions. The purity of $CD14^+$ cells was 96.0% by FACS analysis using an anti-CD14 monoclonal antibody (clone 4C1/CD14; BD Pharmingen). Cells (5×10^5) were injected into the tail vein of syngeneic mice ($n = 7$) at 4 hours after MI.

Statistics

Values are presented as mean ± SEM. Statistical significance was evaluated using unpaired Student's t tests for comparisons between two mean values. Multiple comparisons of more than three groups were performed using analysis of variance, post hoc analyses were performed, and the Bonferroni/Dunn rule was applied. The Kaplan-Meier method was used to estimate survival rates. Mortality was computed with a log-rank test. A value of $p < .05$ was considered significant.

RESULTS

BM Transplantation and G-CSF Mobilization Following MI

The experimental protocol is illustrated in Figure 1A. Single HSCs or whole BM isolated from GFP-transgenic mice was transplanted into irradiated recipient mice; Figure 1B shows the FACS profile. Cells of the $c\text{-}kit^+lineage^-$ accounted for 5.3% ± 1.0% (mean ± SD) of all mononucleated cells (MNCs), whereas $Sca\text{-}1^+CD34^-$ cells constituted 0.65% ± 0.36% of the $c\text{-}kit^+lineage^-$ cells. Tip-SP cells accounted for 30.1% ± 5.4% of the $CD34^-c\text{-}kit^+Sca\text{-}1^+lineage^-$ cells, and HSCs accounted for approximately 0.01% of BM MNCs. The chimeric rate of GFP^+ cells was 94.2% ± 4.1% in the w-BM group ($n = 70$) and 63.3% ± 4.7% in the HSC group ($n = 50$).

MI was induced in a total of 120 mice in three serial independent experiments. Eight mice died during the operation or within 24 hours and were excluded from further analysis. Daily subcutaneous injections of G-CSF (G-CSF(+)) or saline solution (G-CSF(−)) were commenced 24 hours after MI. Forty mice were used for cell division assays (third day) or for determination of infarct size and histological analysis at the acute phase (seventh day), and the remaining 72 mice (44 in the w-BM group and 28 in the HSC group) received subcutaneous injections for 10 days. Nucleated cell counts for peripheral blood were significantly increased by G-CSF in both groups (Fig. 1C).

G-CSF Attenuated Mortality and Improved Cardiac Function After MI

In the w-BM and HSC groups, the G-CSF(+) mice had a lower mortality rate than G-CSF(−) mice (Fig. 2A). There were no significant differences ($p > .05$) in the mortality rates of $G\text{-}CSF^+$ or $G\text{-}CSF^-$ mice between the two groups. The majority of deaths (28 of 33 deaths) happened during the first 10 days; 15 in the

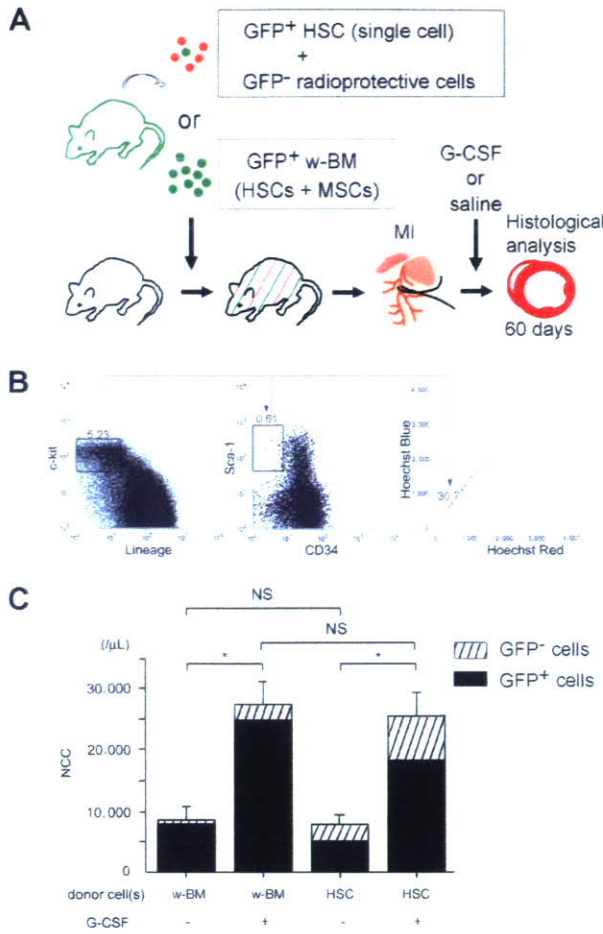

Figure 1. Experimental protocol, isolation of HSCs, and nucleated cell counts in the peripheral blood after G-CSF administration. **(A):** Experimental protocol. Single HSC or whole bone marrow cells from GFP-transgenic mice were transplanted into irradiated mice. A single HSC was injected along with 2×10^5 radioprotected GFP^- BM cells. MI was induced 20 weeks after transplantation, and G-CSF was injected subcutaneously from 24 hours after MI for 10 days. **(B):** Isolation of HSCs from GFP-transgenic mice. Representative results are shown. Cells of the $c\text{-}kit^+lineage^-$ accounted for 5.23% of all mononucleated cells, whereas $Sca\text{-}1^+CD34^-$ cells constituted 0.61% of the $c\text{-}kit^+lineage^-$ cells. Tip-side population cells accounted for 30.7% of the $CD34^-c\text{-}kit^+Sca\text{-}1^+lineage^-$ cells. **(C):** The NCC for peripheral blood samples obtained 24 hours after the last injection of G-CSF or saline. Black columns indicate GFP^+ cells, and striped columns indicate GFP^- cells. *, $p < .0001$. Abbreviations: G-CSF, granulocyte colony-stimulating factor; GFP, green fluorescent protein; HSC, hematopoietic stem cell; MI, myocardial infarction; NCC, nucleated cell counts; NS, not significant; w-BM, whole bone marrow.

w-BM group (4 in the G-CSF(+) and 11 in the G-CSF(−)) and 13 in the HSC group (4 in the G-CSF(+) and 9 in the G-CSF(−)).

In the acute phase, infarct size was not significantly different between the groups (Fig. 2B). However, G-CSF(+) mice in both groups in the chronic phase showed significant improvements in both mean thickness and perimeter of the infarcted area (Fig. 2C, 2D). Echocardiography showed that G-CSF administration was also associated with significant preservation of LV FS, LV EF, and LVEDD in the chronic phase in both groups (Fig. 2E–2G). Hemodynamic measurements confirmed that G-CSF(+) mice had significantly decreased LVEDP, and there was increased LVP and +LVdP/dt in both groups (Fig. 2H–2J). Cardiac function tended to be better in the w-BM groups than the HSC groups, but this difference was not significant. These

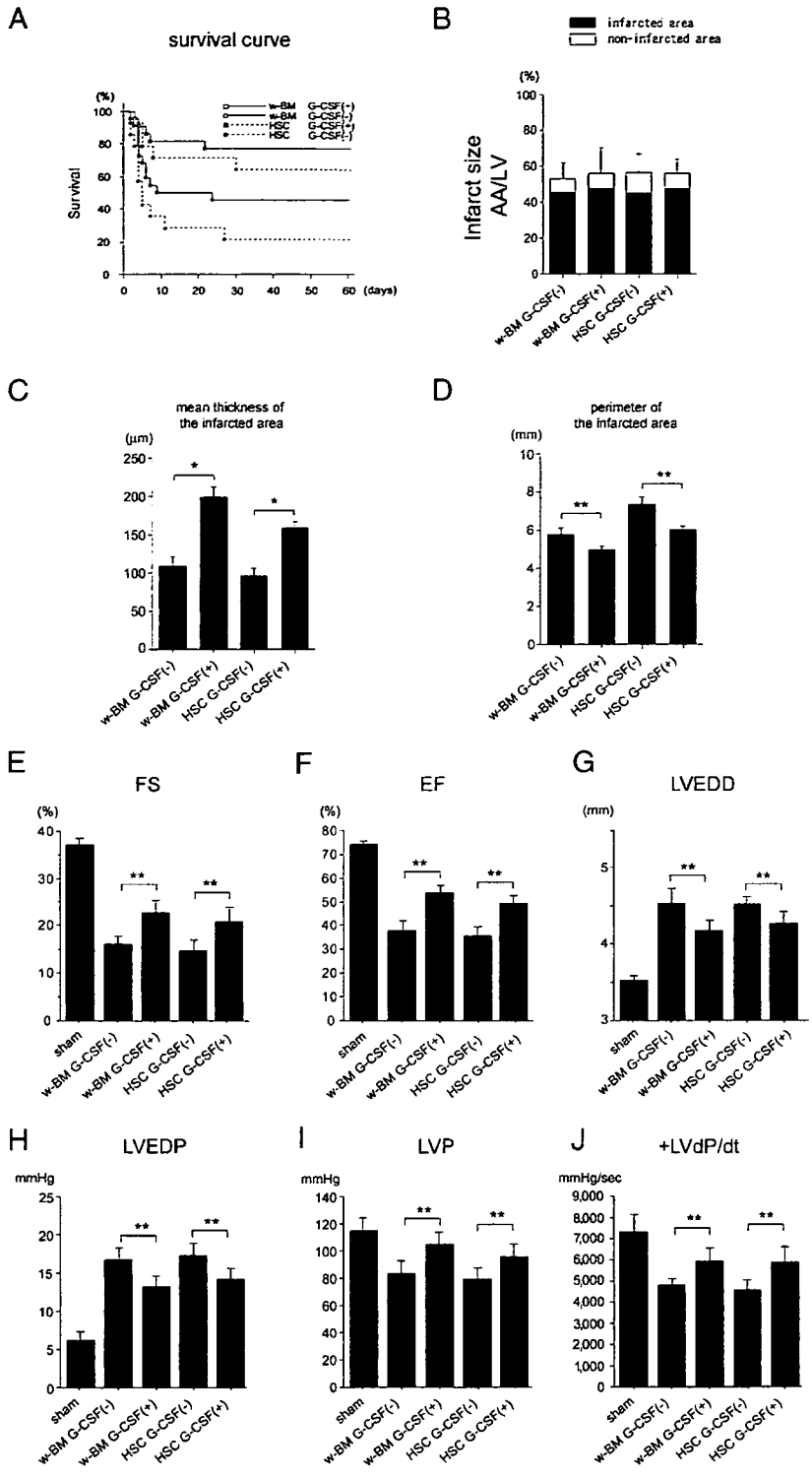

Figure 2. Survival curve, anatomical analysis of the infarcted area, and hemodynamic analysis of cardiac function. **(A):** Survival curve after myocardial infarction in the w-BM- or HSC-transplanted mice with (+) or without (−) G-CSF treatment. G-CSF(+) mice had a lower mortality rate than G-CSF(−) mice ($p < .05$). There were no significant differences in survival rates between w-BM and HSC groups in either G-CSF(+) or G-CSF(−) mice ($p > .05$). **(B):** Infarct size of each group at the acute phase (day 7). Infarct size was not significantly different between groups. **(C–J):** Anatomical and hemodynamic analyses at the chronic phase (day 60). **(C, D):** The mean wall thickness and perimeter of the left ventricle at the papillary muscle level are indicated. **(E–G):** FS, EF, and LVEDD were measured by echocardiography. G-CSF improved FS, EF, and LVEDD in both the w-BM and HSC groups. **(H–J):** A Millar Instruments catheter tip pressure manometer was inserted into the left ventricle to measure LVEDP, LVP, and +LVdP/dt. G-CSF improved LVEDP, LVP, and +LVdP/dt in both the w-BM and HSC groups. *, $p < .01$; **, $p < .05$. Abbreviations: AA, area at risk; EF, ejection fraction; FS, fractional shortening; G-CSF, granulocyte colony-stimulating factor; HSC, hematopoietic stem cell; LV, left ventricular; LVEDD, left ventricular internal end-diastolic diameter; LVEDP, LV end-diastolic pressure; LVP, LV peaked pressure; sec, second; w-BM, whole bone marrow.

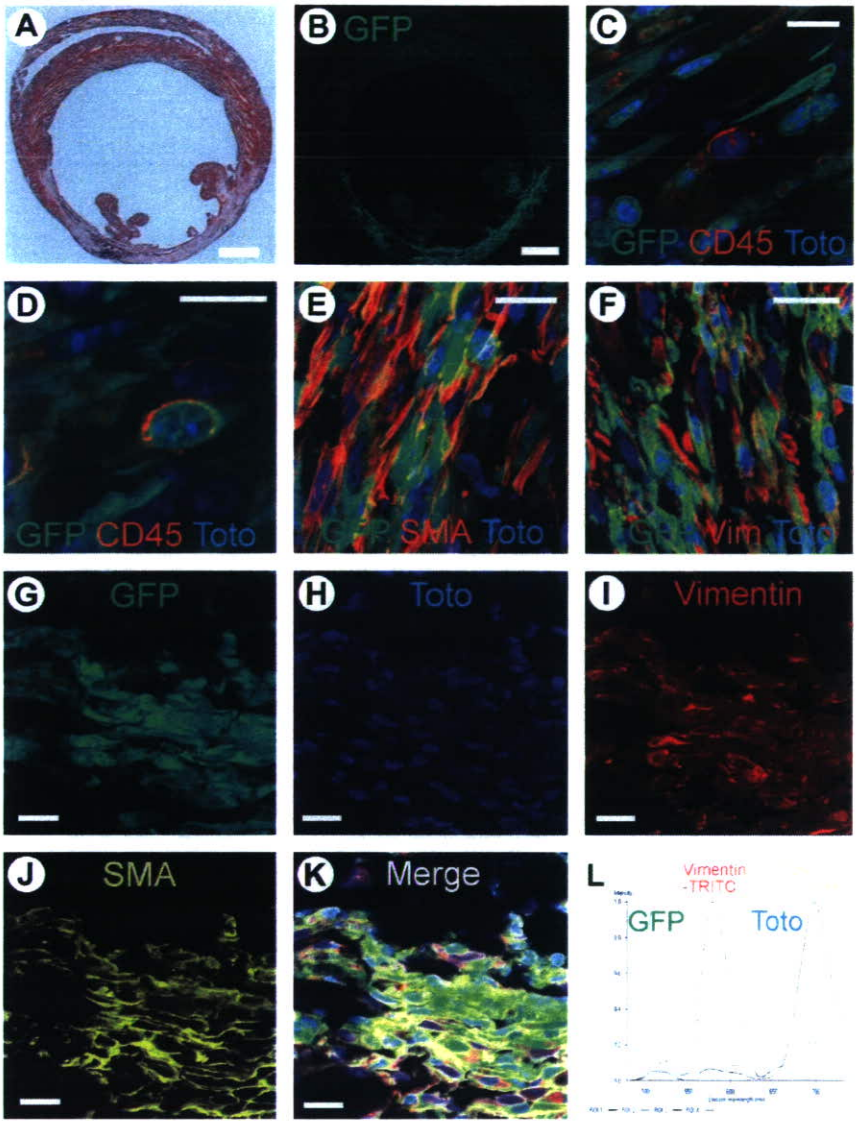

Figure 3. Histological analysis of infarcted hearts in the acute phase after myocardial infarction (MI). **(A, B):** Serial sections of the infarcted heart of the G-CSF(+) hematopoietic stem cell group at the acute phase (day 7) after MI with Azan staining **(A)** and immunofluorescence **(B)**. Note that GFP was strongly expressed in the infarcted area. Scale bars = 1 mm. **(C, D):** Although whole round BM-derived GFP^+ cells were strongly positive for CD45, most of the elongated fibroblast-like GFP cells were negative for CD45. Green, red, and blue signals indicate GFP, CD45, and TOTO-3, respectively. Scale bars = 10 μm. **(E, F):** Most of the elongated GFP^+ fibroblast-like cells were positive for both α-SMA and Vim, indicating that they are myofibroblasts. Green, red, and blue signals indicate GFP, α-SMA **(E)** or Vim **(F)** and TOTO-3, respectively. Scale bars = 20 μm. **(G–L):** Quadruple immunostaining was performed on the LSM510 META. **(G–K):** GFP cells in the infarcted area expressed both Vim and α-SMA. **(L):** emission spectrum for each dye. Scale bars = 20 μm. Abbreviations: GFP, green fluorescent protein; SMA, smooth muscle actin; TRITC, tetramethylrhodamine B isothiocyanate; Vim, vimentin.

findings indicate that G-CSF administration decreased mortality following MI in both groups and that this effect was associated with improved cardiac function and remodeling.

G-CSF Increased HSC-Derived Myofibroblasts at the Infarcted Area in the Acute Phase

To investigate the mechanism by which cardiac remodeling, function, and survival were improved in the G-CSF(+) mice, we examined the infarcted region by histochemistry at day 7. Strong GFP signals were observed in the infarcted area of the G-CSF(+) HSC group (Fig. 3A, 3B). Triple staining revealed infiltrating GFP^+CD45^+ hematopoietic cells and a number of $GFP^+CD45^{low/-}$ fibroblast-like elongated cells in the infarcted area (Fig. 3C, 3D). The GFP^+ fibroblast-like cells also stained positive for vimentin and α-SMA (Fig. 3E, 3F). Quadruple staining confirmed that the fibroblast-like GFP^+ cells simultaneously expressed both vimentin and α-SMA, suggesting they were myofibroblasts of hematopoietic origin (Fig. 3G–3L).

Azan staining showed a thin and elongated infarct area in all G-CSF(+) and G-CSF(−) mice of the w-BM and HSC groups, although there were no significant differences in LV dimensions or remodeling between them at this stage (Fig. 4A–4D). Quantitative analysis revealed, however, that G-CSF significantly augmented the number of GFP^+ cells more than threefold in both groups (Fig. 4E–4H, 4Q). Although there were fewer GFP^+ cells in the HSC group than in the w-BM group, it was not possible to directly compare them because of different chimeric rates between the two groups. Triple staining confirmed that G-CSF administration significantly increased the number of BM-derived myofibroblasts in the infarcted area for both groups (Fig. 4I–4P, 4R, 4S). Quantitative analysis of the BM-derived (GFP^+) and intrinsic (GFP^-) myofibroblasts also showed that G-CSF markedly augmented the BM-derived population (Fig. 4T). These results suggested that administration of G-CSF promotes myofibroblast-rich repair by recruiting BM-derived cells in the acute phase.

G-CSF Increased HSC-Derived Fibroblasts at the Infarcted Area in the Chronic Phase

Next, we examined the histology of infarcted hearts in the chronic phase at 60 days post-MI. At low magnification, GFP^+ cells were visible in the infarcted area of both w-BM and HSC groups (supplemental online Fig. 1A, 1B; data not shown). High-magnification images revealed GFP^+ elongated cells pos-

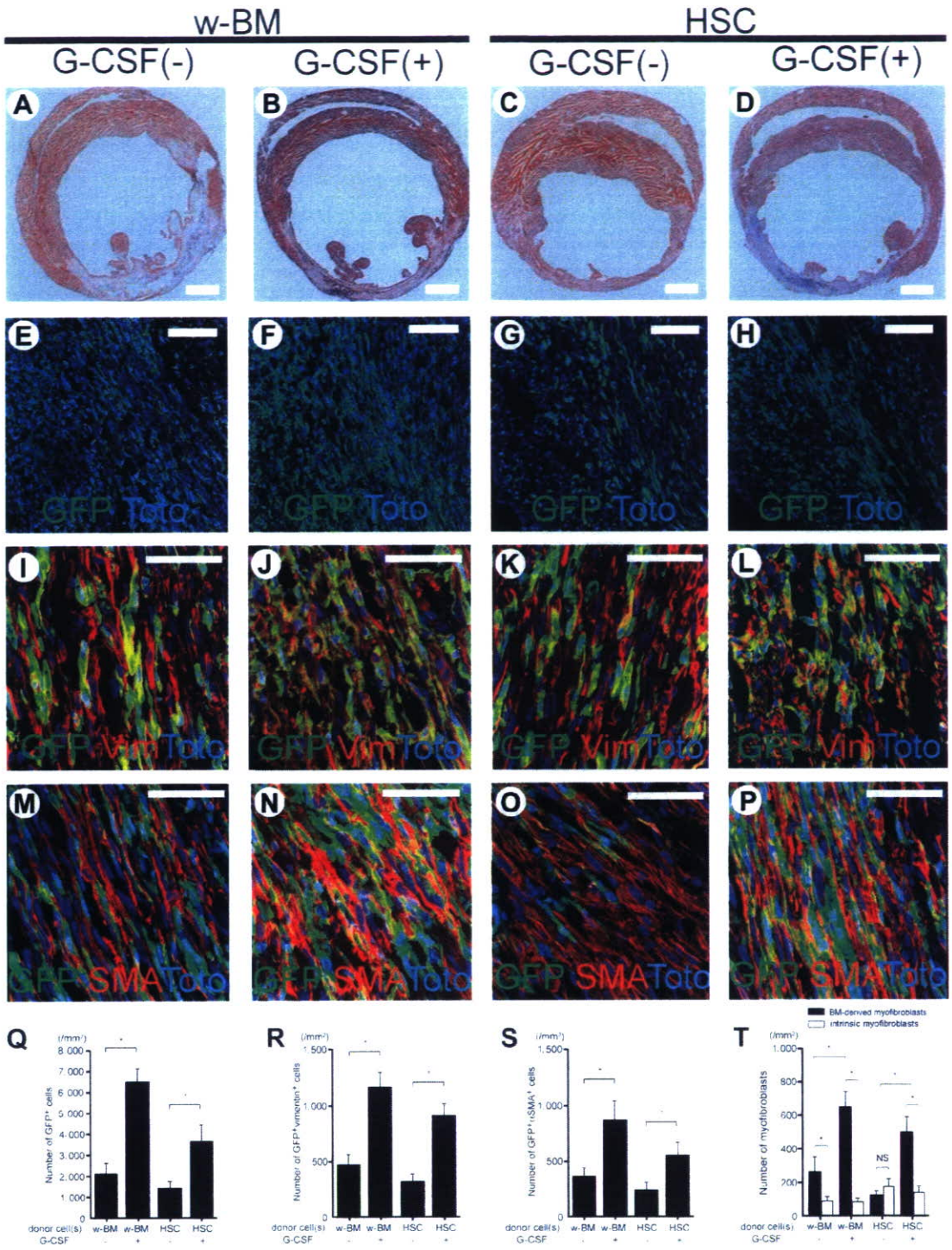

Figure 4. Quantitative analysis of GFP^+ cells and GFP myofibroblasts in the acute-phase infarct area. **(A–D):** Azan staining of the infarcted hearts at day 7 after MI. Scale bars = 1 mm. **(E–H):** GFP^+ cells in the infarcted area. Green and blue signals indicate GFP and TOTO-3, respectively. Scale bars = 100 μm. **(I–L):** GFP^+Vim^+ cells in the infarct area. Green, red, and blue signals indicate GFP, Vim, and TOTO-3, respectively. Scale bars = 50 μm. **(M–P):** $GFP^-\alpha$-SMA^- cells in the infarcted area. Green, red, and blue signals indicate GFP, α-SMA, and TOTO-3, respectively. Scale bars = 50 μm. **(Q–S):** Quantitative analysis of GFP^+ cells **(Q)**, GFP^+Vim^+ cells **(R)**, and $GFP^+\alpha$-SMA^+ cells **(S)** in the infarcted area. **(T):** Quantitative analysis of the BM-derived (GFP^-) and intrinsic (GFP^-) myofibroblasts in the infarcted area. The number of cells was scored using 100 specimens per group of mice. *, $p < .01$. Abbreviations: BM, bone marrow; G-CSF, granulocyte colony-stimulating factor; GFP, green fluorescent protein; HSC, hematopoietic stem cell; NS, not significant; SMA, smooth muscle actin; Vim, vimentin; w-BM, whole bone marrow.

itive for vimentin (supplemental online Fig. 1C, 1D) but not CD45 (data not shown). Emission fingerprinting confirmed that the signal was consistent with GFP emission and not nonspecific autofluorescence (supplemental online Fig. 1E, 1F).

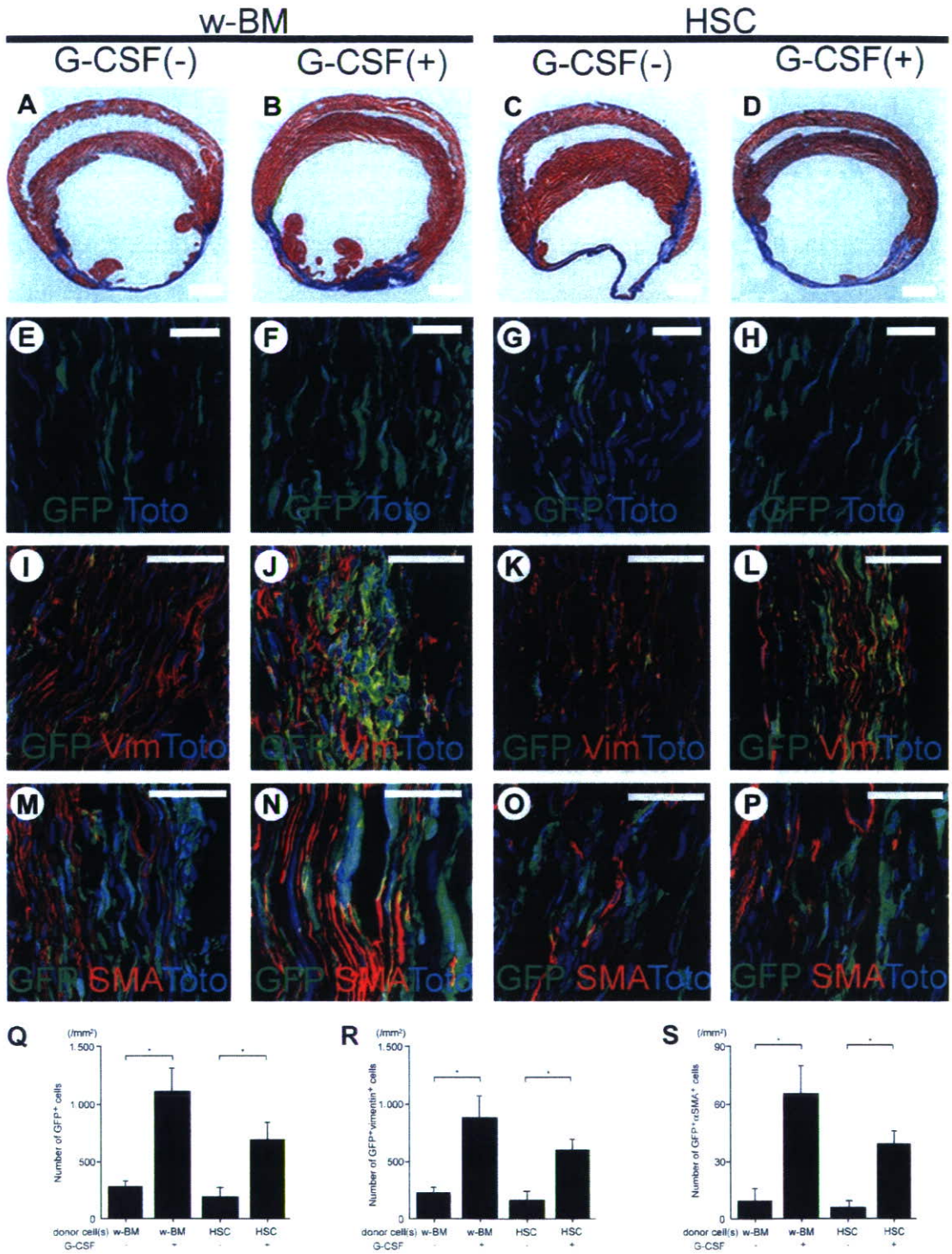

Figure 5. Quantitative analysis of the GFP$^+$ cells and GFP$^+$ myofibroblasts in the chronic-phase infarct area. **(A–D):** Azan staining of the infarcted hearts at day 60 after myocardial infarction obtained from G-CSF(−) and G-CSF(+) mice in the w-BM and HSC groups. Scale bars = 1 mm. **(E–H):** GFP$^-$ cells in the infarcted area. The morphology of most GFP$^-$ cells was elongated and narrow rather than spherical. Green and blue signals indicate GFP and TOTO-3, respectively. Scale bars = 50 μm. **(I–L):** GFP$^-$vimentin$^-$ cells in the infarcted area. Green, red, and blue signals indicate GFP, vimentin, and TOTO-3, respectively. Scale bars = 50 μm. **(M–P):** GFP$^-$ α-SMA$^+$ cells in the infarcted area. Green, red, and blue signals indicate GFP, α-SMA, and TOTO-3, respectively. Scale bars = 20 μm. **(Q–S):** Quantitative analysis of GFP$^+$ cells **(Q)**, GFP$^+$vimentin$^+$ cells **(R)**, and GFP$^-$ α-SMA$^+$ cells **(S)** in the infarcted area. The number of cells was scored in 100 specimens per group of mice. *, $p < .01$. Abbreviations: G-CSF, granulocyte colony-stimulating factor; GFP, green fluorescent protein; HSC, hematopoietic stem cell; NS, not significant; SMA, smooth muscle actin; vWF, von Willebrand factor; w-BM, whole bone marrow.

In both w-BM and HSC groups, the infarcted area was thin and elongated, and the left ventricle was enlarged, indicating that cardiac remodeling had occurred (Fig. 5A–5D). Cardiac remodeling tended to be more prominent in the animals that did

not receive G-CSF (Fig. 5A, 5C). GFP^+ cells were observed at the infarcted area (Fig. 5E–5H), and G-CSF significantly augmented the number of GFP^+ cells at this site (Fig. 5Q). Costaining for vimentin identified elongated GFP^+ vimentin$^+$ cells (Fig. 5I–5L), which were increased by G-CSF in both w-BM and HSC groups (Fig. 5R). However, costaining with α-SMA showed only a small number of GFP^+ α-SMA^+ cells in the infarcted area (Fig. 5M–5P), although the G-CSF(+) mice had more of these cells than the G-CSF(−) mice in both groups (Fig. 5S). These results suggested that the HSC-derived myofibroblasts observed in the acute phase became α-SMA^- fibroblasts by the chronic phase.

Regeneration of Vascular Cells and Cardiomyocytes by BM-Derived Cells

Immunostaining of G-CSF(+) mice in the w-BM group revealed that some GFP^+ cells were vWF^+, whereas others were α-SMA^+ and integrated into the microvessels (Fig. 6A, 6B). These findings were not replicated in the other mouse groups, suggesting that administration of G-CSF also mobilized endothelial cells and smooth muscle cells from BM and that these cells contributed to the vascular regeneration.

Triple staining for GFP, actinin, and TOTO-3 revealed GFP^+ cardiomyocytes, which showed clearly defined striations (Fig. 6C–6E) only in the w-BM groups (Fig. 6F). This suggested that MSCs were also mobilized by G-CSF administration and subsequently differentiated into cardiomyocytes, as described previously [6]. G-CSF administration significantly increased the numbers of these cells (Fig. 6F).

To examine whether G-CSF also increased the number of proliferating cardiomyocytes in the noninfarcted area, we performed immunostaining for Ki-67 at days 3 and 7 after MI in the w-BM groups. Approximately 0.5% of cardiomyocytes were positive for Ki67 at day 3, and this number was unaffected by G-CSF treatment, indicating that the hemodynamic improvement mediated by G-CSF was not due to cardiomyocyte proliferation (Fig. 6G, 6H).

Intravenously Injected Murine Monocytes Differentiated into Myofibroblasts in the Infarcted Area

Finally, based on reports that macrophages injected into infarcted hearts promote myofibroblast accumulation [8], we speculated that peripheral blood monocytes could be the precursors of the HSC-derived cardiac myofibroblasts. We isolated monocytes from the peripheral blood of G-CSF-stimulated GFP-transgenic mice and injected them into the tail vein of syngeneic mice at 4 hours after MI. Immunofluorescent staining at day 60 revealed GFP^+ cells in the infarct area (Fig. 7A). High magnification further showed the elongated GFP^+ cells expressing both vimentin and α-SMA, indicating differentiation into cardiac myofibroblasts in the infarcted area (Fig. 7B–7F).

DISCUSSION

This study first demonstrated that cardiac myofibroblasts derive from HSCs and that G-CSF markedly increases the number of HSC-derived myofibroblasts in an infarcted area in murine hearts. The study further indicated peripheral blood monocytes as precursors of the cardiac myofibroblasts. It has been reported that myofibroblast-rich tissue mediates infarcted segment stabilization after MI and contributes to scar thickening to reduce ventricular wall stress, prevent infarct

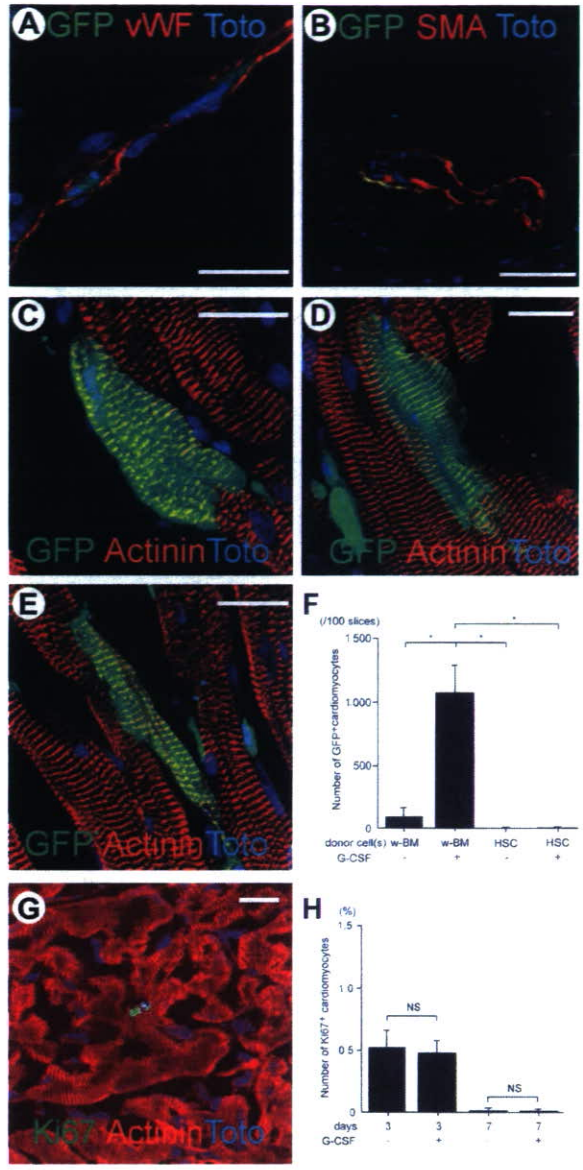

Figure 6. Vascular and myocardial regeneration by bone marrow (BM)-derived cells and analysis of cardiomyocyte cell division. **(A, B):** Vascular regeneration by BM-derived cells at day 60 after myocardial infarction (MI) in G-CSF(+) mice of the w-BM group. Immunofluorescent staining revealed GFP^+ endothelial **(A)** and smooth muscle cells in the vascular structure **(B)**. Green, red, and blue signals indicate GFP, von Willebrand factor **(A)** or α-SMA **(B)**, and TOTO-3, respectively. Scale bars = 50 μm, respectively. **(C–F):** Myocardial regeneration by BM-derived cells at day 60 after MI in G-CSF(+) mice of the w-BM group. **(C–E):** GFP^+ actinin$^+$ cardiomyocytes found in the G-CSF(+) mice of the w-BM group. GFP^+actinin$^+$ cells showed typical striations. Green, red, and blue signals indicate GFP, actinin, and TOTO-3, respectively. Scale bars = 20 μm, respectively. **(F):** Quantitative analysis of GFP^+actinin$^+$ cells in the infarcted area. The number of cells was scored using 100 specimens per group of mice. *, $p < .0001$. **(G, H):** Effect of G-CSF on cardiomyocyte proliferation. **(G):** Immunofluorescence image of a cardiomyocyte expressing Ki67 in a G-CSF(+) mouse at day 3 after MI. Green, red, and blue signals indicate Ki67, actinin, and TOTO-3, respectively. Scale bar = 20 μm. **(H):** Quantitative analysis of $Ki67^+$ cardiomyocytes in the noninfarcted area at days 3 and 7 after MI. The number of cells was scored in 100 specimens per group of mice. Abbreviations: G-CSF, granulocyte colony-stimulating factor; GFP, green fluorescent protein; HSC, hematopoietic stem cell; NS, not significant; SMA, smooth muscle actin; vWF, von Willebrand factor; w-BM, whole bone marrow.

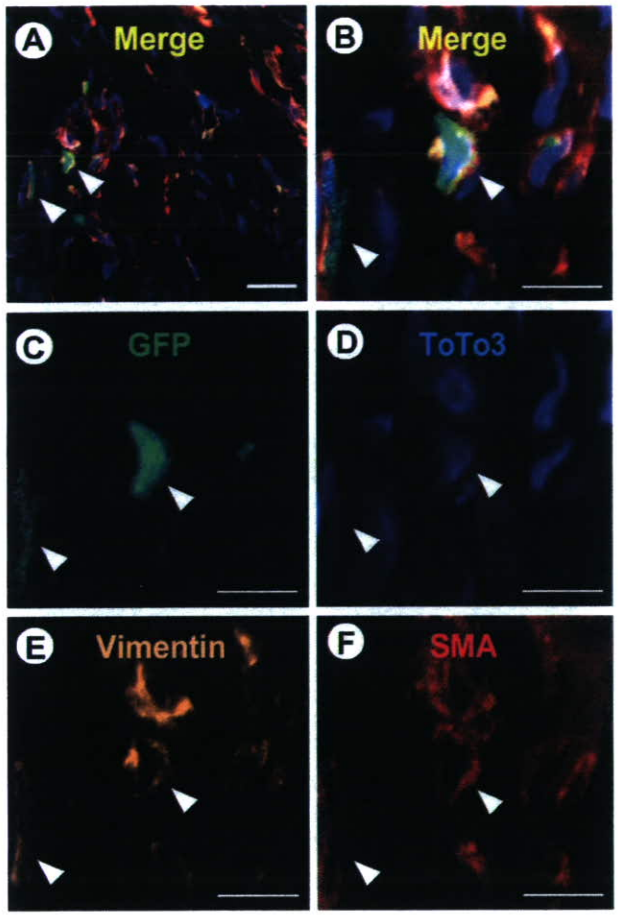

Figure 7. The monocyte fraction can differentiate into myofibroblasts in the infarcted area. The monocyte fraction isolated from GFP-transgenic mice was injected into the tail vein of syngeneic mice that had undergone MI. **(A):** Immunofluorescent staining revealed GFP$^+$ cells in the infarcted area at day 60 after MI. **(B–F):** High magnification revealed that GFP$^+$ cells **(C)** expressed TOTO-3 **(D)**, vimentin **(E)**, and α-SMA **(F)**, indicating they were myofibroblasts. In each panel, green, red, orange, and blue signals indicate GFP, actinin, α-SMA, and TOTO-3, respectively. Scale bars = 20 μm **(A)** and 10 μm **(B–F)**. Abbreviations: GFP, green fluorescent protein; SMA, smooth muscle actin.

expansion, and improve cardiac function [7, 8, 14]. In the present study, taken together with the improvements in thickness and perimeter of the infarcted area and the improved post-MI function of G-CSF(+) mice, it was strongly suggested that administration of G-CSF enhances cardiac repair by promoting HSC-derived myofibroblast-rich scar formation. We propose the following mechanism for G-CSF-mediated cardiac repair. First, MI recruits peripheral blood monocytes to the infarct area, and this accumulation is further enhanced by G-CSF by mobilizing monocytes from BM into the blood circulation. Although the majority of circulating murine monocytes generally migrate into tissues within 32 hours (half blood transit time = 22 hours) even at steady state, the blood transit time is further shortened in acute inflammatory states [15]. Therefore, the BM-derived monocytes should have also migrated into the ischemic myocardium within a short time after MI. Monocytes/macrophages in the infarct area then differentiate into myofibroblasts and contribute to scar thickening, resulting in cardiac protection in the acute phase. Finally, activated myofibroblasts transform back into their resting fibroblastic form in the chronic phase. The mobilized monocytes/macrophages might also activate matrix metalloproteinases, release chemokines, and phagocytose necrotic tissue in the acute phase, further promoting the healing process. It is clear, however, that intrinsic (GFP$^-$) myofibroblasts/fibroblasts also contribute to the healing process, possibly by moving from the BM to the myocardial tissue as macrophages or c-kit$^+$ cells prior to the transplantation of BM cells. We know this from previous work showing that BM-derived macrophages and HSCs exist in steady-state murine muscle tissue [16].

Myofibroblasts/fibroblasts exist in many organs and participate in a range of pathophysiological processes. Recently, BM-derived myofibroblasts have been identified in various tissues following radiation injury, including the lung, stomach, skin, kidney, and esophagus [17], as well as in the fibrotic tissues of liver cirrhosis [18]. We also previously reported that BM-derived cells can mobilize to hypertensive pulmonary arteries and differentiate into myofibroblasts in hypoxia-induced pulmonary hypertensive mice [19]. Ogawa et al. also demonstrated that myofibroblasts/fibroblasts in several other organs/tissues, including murine heart valves, derive from HSCs by a clonal study [20]. Accordingly, the present study further examined the origin of BM-derived myofibroblasts/fibroblasts in a murine MI model. Future studies need to determine the derivation of many other myofibroblast/fibroblast populations, as well as the effects, beneficial or otherwise, of G-CSF administration at the sites where these populations reside.

Interestingly, G-CSF also promoted myocardial and vascular regeneration by BM-derived cells, suggesting that G-CSF simultaneously recruits plural BM stem cells (i.e., HSCs, MSCs, and endothelial progenitor cells) or their descendants for tissue repair. Although fusion of hematopoietic cells and cardiomyocytes was recently proposed as a mechanism for cardiac regeneration by BM-derived cells [21], we previously demonstrated that BM-derived MSCs could differentiate into cardiomyocytes in vitro, and those cells could be mobilized into ischemic myocardium in vivo [6, 22]. Furthermore, it was reported that monocytes obtained from murine peripheral blood could differentiate into fibroblasts in vitro [23]. We also confirmed that monocytes obtained from adult human peripheral blood differentiate into fibroblasts without cell fusion in vitro (unpublished observation). Therefore, we believe that (trans)differentiation of plural BM-derived stem cells also plays an important role in G-CSF-mediated cardiac repair after MI. Furthermore, recent findings showed that G-CSF also directly binds G-CSF receptors on cardiomyocytes, activating the JAK/STAT pathway and preventing apoptosis in the late phase after MI, thereby improving cardiac remodeling [4]. These effects may have also contributed to the improved cardiac function by G-CSF observed in our study. Although administration of G-CSF has improved function and/or survival in rodent MI models, similar effects in humans remain controversial [24]. We speculate that the time needed for cardiac remodeling in humans compared with rodents is a critical point in this discussion. Our finding that human peripheral blood monocytes could also become myofibroblasts/fibroblasts in vitro and in the infarcted myocardium of immunodeficient mice promoting cardiac repair (unpublished observation) hints that an appropriate administration of G-CSF would also be beneficial in humans following MI.

ACKNOWLEDGMENTS

This work was supported by grants from the Ministry of Education, Science and Culture of Japan; the Ministry of Welfare and Labor of Japan; the Japan Health Science Foundation; the Vehicle Racing Commemorative Foundation; and the 21st Century COE Program of the Ministry of Education, Science and Culture of Japan. J. Fujita, M. Mori, and H. Kawada contributed equally to this work.

DISCLOSURE OF POTENTIAL CONFLICTS OF INTEREST

The authors indicate no potential conflicts of interest.

REFERENCES

1 Orlic D, Kajstura J, Chimenti S et al. Bone marrow cells regenerate infarcted myocardium. Nature 2001;410:701–705.
2 Schachinger V, Assmus B, Britten MB et al. Transplantation of progenitor cells and regeneration enhancement in acute myocardial infarction: Final one-year results of the TOPCARE-AMI Trial. J Am Coll Cardiol 2004;44:1690–1699.
3 Kang H-J, Kim H-S, Zhang S-Y et al. Effects of intracoronary infusion of peripheral blood stem-cells mobilised with granulocyte-colony stimulating factor on left ventricular systolic function and restenosis after coronary stenting in myocardial infarction: The MAGIC cell randomised clinical trial. Lancet 2004;363:751–756.
4 Harada M, Qin Y, Takano H et al. G-CSF prevents cardiac remodeling after myocardial infarction by activating the Jak-Stat pathway in cardiomyocytes. Nat Med 2005;11:305–311.
5 Orlic D, Kajstura J, Chimenti S et al. Mobilized bone marrow cells repair the infarcted heart, improving function and survival. Proc Natl Acad Sci U S A 2001;98:10344–10349.
6 Kawada H, Fujita J, Kinjo K et al. Nonhematopoietic mesenchymal stem cells can be mobilized and differentiate into cardiomyocytes after myocardial infarction. Blood 2004;104:3581–3587.
7 Fazel S, Cimini M, Chen L et al. Cardioprotective c-kit+ cells are from the bone marrow and regulate the myocardial balance of angiogenic cytokines. J Clin Invest 2006;116:1865–1877.
8 Leor J, Rozen L, Zuloff-Shani A et al. Ex vivo activated human macrophages improve healing, remodeling, and function of the infarcted heart. Circulation 2006;114(1 suppl):I94–I100.
9 Okabe M, Ikawa M, Kominami K et al. 'Green mice' as a source of ubiquitous green cells. FEBS Lett 1997;407:313–319.
10 Matsuzaki Y, Kinjo K, Mulligan RC et al. Unexpectedly efficient homing capacity of purified murine hematopoietic stem cells. Immunity 2004;20:87–93.
11 Osawa M, Hanada K, Hamada H et al. Long-term lymphohematopoietic reconstitution by a single CD34-low/negative hematopoietic stem cell. Science 1996;273:242–245.
12 Sahn D, DeMaria A, Kisslo J et al. Recommendations regarding quantitation in M-mode echocardiography: Results of a survey of echocardiographic measurements. Circulation 1978;58:1072–1083.
13 Michael LH, Entman ML, Hartley CJ et al. Myocardial ischemia and reperfusion: A murine model. Am J Physiol 1995;269:H2147–H2154.
14 Virag JI, Murry CE. Myofibroblast and endothelial cell proliferation during murine myocardial infarct repair. Am J Pathol 2003;163:2433–2440.
15 van Furth R, Thompson J, Gassmann AE. The kinetics of mononuclear phagocytes during normal steady-state conditions, acute inflammation, and the effect of glucocorticosteroids and azathioprine (Imuran). In: Braun W, Ungar J, eds."Nonspecific" Factors Influencing Host Resistance. Basel: S. Karger, 1973:79–94.
16 Kawada H, Ogawa M. Bone marrow origin of hematopoietic progenitors and stem cells in murine muscle. Blood 2001;98:2008–2013.
17 Direkze NC, Forbes SJ, Brittan M et al. Multiple organ engraftment by bone-marrow-derived myofibroblasts and fibroblasts in bone-marrow-transplanted mice. STEM CELLS 2003;21:514–520.
18 Forbes SJ, Russo FP, Rey V et al. A significant proportion of myofibroblasts are of bone marrow origin in human liver fibrosis. Gastroenterology 2004;126:955–963.
19 Hayashida K, Fujita J, Miyake Y et al. Bone marrow-derived cells contribute to pulmonary vascular remodeling in hypoxia-induced pulmonary hypertension. Chest 2005;127:1793–1798.
20 Ogawa M, LaRue AC, Drake CJ. Hematopoietic origin of fibroblasts/myofibroblasts: Its pathophysiologic implications. Blood 2006;108:2893–2896.
21 Zhang S, Shpall E, Willerson JT et al. Fusion of human hematopoietic progenitor cells and murine cardiomyocytes is mediated by $\alpha 4\beta 1$ integrin/vascular cell adhesion molecule-1 interaction. Circ Res 2007;100:693–702.
22 Makino S, Fukuda K, Miyoshi S et al. Cardiomyocytes can be generated from marrow stromal cells in vitro. J Clin Invest 1999;103:697–705.
23 Ebihara Y, Masuya M, Larue AC et al. Hematopoietic origins of fibroblasts: II. In vitro studies of fibroblasts, CFU-F, and fibrocytes. Exp Hematol 2006;34:219–229.
24 Schabitz W-R, Nikol S, Schneider A. Granulocyte colony-stimulating factor and acute myocardial infarction. JAMA 2006;296:1967–1968.

See www.StemCells.com for supplemental material available online.

Use of an epidural cooling catheter with a closed countercurrent lumen to protect against ischemic spinal cord injury in pigs

Akihiro Yoshitake, MD,[a] Atsuo Mori, MD,[c] Hideyuki Shimizu, MD,[a] Toshihiko Ueda, MD,[a] Nobuyuki Kabei, PhD,[c] Takashi Hachiya, MD,[c] Hideyuki Okano, MD,[b] and Ryohei Yozu, MD[a]

Drs Yozu, Yoshitake, Mori, and Kabei (*left to right*)

CSP

Objective: We developed an epidural cooling catheter containing cold saline solution circulating in an isolated lumen. After placement by a minimally invasive approach, we evaluated protection effect against ischemic spinal cord injury in pigs.

Methods: Fourteen pigs underwent thoracic aortic double clamping for 45 minutes under systemic mild hypothermia (36°C). Group A (n = 7) underwent local hypothermia with the cooling catheter. Group B (n = 7) underwent catheter placement only, without cooling. Spinal cord somatosensory evoked potentials were recorded to assess electrophysiologic status. Neurologic function was evaluated with a modified Tarlov score.

Results: At aortic crossclamping, spinal temperature in group A (26.5°C ± 2.4°C) was significantly lower than that in group B (35.3°C ± 0.6°C, $P = .0001$). Mean time from aortic crossclamping to onset of potential loss was significantly longer in group A (28.4 ± 6.6 minutes) than in group B (18.3 ± 5.0 minutes, $P = .007$). Mean duration of total loss of potentials was significantly shorter in group A (19.0 ± 6.7 minutes) than that in group B (31.3 ± 5.9 minutes, $P = .003$). Group A showed significantly better neurologic function (mean Tarlov score 4.4 ± 0.8) than that of group B (0.1 ± 0.4, $P = .0001$). Mean total number of intact motor neurons was significantly greater in group A (24.5 ± 6.8) than that of group B (9.9 ± 6.8, $P = .0001$).

Conclusion: By cooling the spinal cord selectively and continuously, the newly designed epidural cooling catheter prevented ischemic injury in a pig model of aortic crossclamping.

From the Departments of Cardiovascular Surgery[a] and Physiology,[b] Keio University School of Medicine, Tokyo, Japan; and the Department of Cardiovascular Surgery,[c] Saitama Cardiovascular and Respiratory Center, Osatogun, Japan.

Supported by the scientific research fund of Saitama prefecture.

Received for publication April 22, 2007; revisions received May 27, 2007; accepted for publication June 11, 2007.

Address for reprints: Akihiro Yoshitake, MD, Department of Cardiovascular Surgery, Keio University School of Medicine, 35 Shinanomachi, Shinjuku, Tokyo, Japan (E-mail: akihiro197253@yahoo.co.jp).

J Thorac Cardiovasc Surg 2007;134:1220-6

0022-5223/$32.00

doi:10.1016/j.jtcvs.2007.06.015

Paraplegia has remained a devastating problem associated with thoracoabdominal aneurysm repair. Reported incidence of this complication ranges from 5% to 8% in advanced centers.[1-4] Numerous surgical and pharmacologic interventions have been proposed for prevention, but no single method has succeeded completely in avoiding this dreaded complication.

Systemic hypothermia is a protective measure used frequently against paraplegia associated with aortic surgery.[5-7] It carries, however, risks of coagulopathy, pulmonary dysfunction, and cardiac arrhythmia.

Regional hypothermia would be a logical alternative approach to minimizing adverse effects of systemic hypothermia while preserving its merits.[8] Cambria and colleagues[9] reported a method of regional cooling involving infusion of iced saline solution into the epidural space, demonstrating that infused iced saline solution without drainage from the epidural space could cool the spinal cord selectively. This method raised the major concern of possible associated eleva-

Abbreviations and Acronyms
sSEP = spinal cord somatosensory evoked potential

tion in cerebrospinal fluid pressure, however, which would worsen spinal cord perfusion.[10]

In a previous experimental study, we examined the effectiveness of epidural cooling against spinal cord ischemia by simply placing a U-shaped catheter containing cold circulating saline solution in the epidural space.[11] This protocol required two large skin incisions (70 mm) and open laminectomy to permit catheter introduction, however, making the procedure too invasive for clinical use.

To overcome this problem, we developed a new cooling catheter with a closed countercurrent lumen. This less cumbersome catheter could be placed with only minimal invasiveness. We investigated its cooling ability and protection against ischemic injury in pigs.

Materials and Methods

All animals received humane care and treatment in accordance with the "Guide for the Care and Use of Laboratory Animals" (www.nap.edu/catalog/5140.html). Further, both the experimental and animal care protocols were approved by the Animal Care Committee of Saitama Cardiovascular and Respiratory Center, Osatogun, Japan.

Epidural Cooling Catheter and Continuous Cord Cooling System

The basic concept of our cooling system has been reported previously.[11] In this study, saline solution was cooled externally to 4°C and circulated at a constant rate of 45 mL/min by an external pump (AST Co, Ltd, Higashimatsuyama, Japan). Instead of placing a loop catheter bent at the midpoint to form a U shape, we developed a special catheter with a closed countercurrent lumen. This polyurethane cooling catheter (Unitika, Tokyo, Japan), with a 16-gauge outer diameter and 25 cm length, had a lumen in which cold saline solution could circulate without leakage (Figure 1). The coolant entered the inlet limb of the cooling catheter, passed through the full length of the lumen, and then turned back at the tip of the catheter to be returned to the external units.

Surgical Preparation, Catheter Installation, and Cooling Protocol

A total of 14 adult pigs weighting 35 to 40 kg were used. The animals were randomly divided into two equal groups, a regional hypothermia group with cold saline solution circulating through the epidural cooling catheter (group A) and a control group with catheter placement but no circulating cold saline solution (group B).

Swine were anesthetized initially with intramuscular ketamine (15 mg/kg), intubated, and placed in a right lateral decubitus position on a cooling-warming blanket to maintain mild systemic hypothermia (36°C). Anesthesia was maintained with 2.0% isoflurane added to a mixture of 50% oxygen and 50% nitrous oxide.

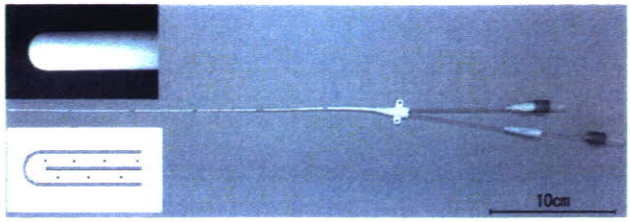

Figure 1. Epidural countercurrent cooling catheter. Saline solution circulates in isolated lumen of cooling catheter, reversing flow direction at tip of catheter without epidural leakage.

A 30-mm vertically oriented incision was made 10 mm lateral to the midline at the level of L3. According to a minimally invasive technique used in orthopedics (METRx-MD; Medtronic Sofamor Danek, Minneapolis, Minn), the caudal part of the superior lamina and the ligamentum flavum were exposed.[12] Partial caudal hemilaminectomy and removal of the ligamentum flavum were performed to provide entry for the tip of the epidural cooling catheter. Under fluoroscopic guidance, the catheter was advanced carefully into the dorsal epidural space in a cephalad direction until the tip reached the level of Th6. Proximal epidural temperature, distal epidural temperature, and spinal temperature were recorded continuously with thermistor probes placed upon the dorsal dura at Th5 and L4 and in the subarachnoid space at L4. An intrathecal pressure sensor (Johnson & Johnson, Raynham, Mass) was introduced into the subarachnoid space by means of needle puncture at the L5-L6 interspace.

Left thoracotomy was performed at both the fourth and seventh interspaces. Systemic anticoagulation was provided with heparin sulfate (6-U/kg intravenous bolus). Pressure monitoring catheters were inserted into the right axillary artery, the middle portion of the crossclamped descending thoracic aorta, and the right femoral artery for recording of arterial pressures proximal, central, and distal to the aortic crossclamp, respectively. In both groups swine underwent thoracic double aortic crossclamping for 45 minutes distal to the origin of the left subclavian artery and also just above the diaphragm (Figure 2). During aortic crossclamping, proximal hypertension was controlled with nicardipine hydrochloride (4 μg/kg as bolus). After aortic unclamping, blood pressure was restored with phenylephrine hydrochloride (3 μg/kg as bolus).

Group A animals underwent epidural cooling with the cooling catheter, beginning 30 minutes before aortic crossclamping and continuing during the 45 minutes of aortic crossclamping. After clamp release, epidural cooling was continued for 30 further minutes to slow the rise of spinal temperature accompanying reperfusion (total epidural cooling 105 minutes). In group B, the epidural catheter was placed in the same fashion, but swine did not undergo epidural cooling at any point in the procedure. After surgery, pigs were extubated and returned to cages with free access to water and food.

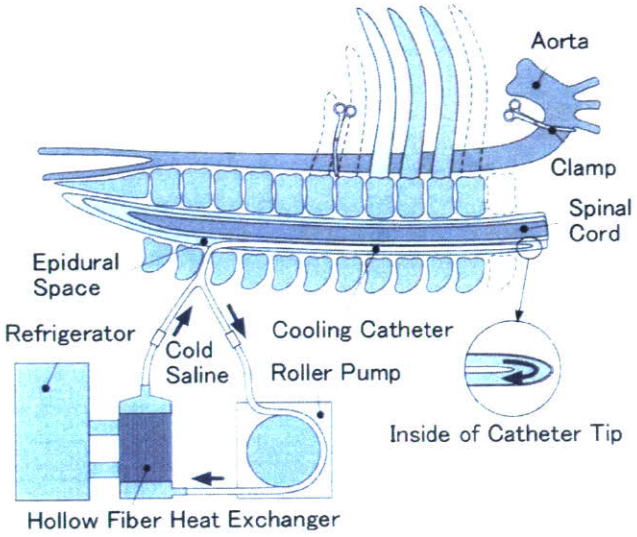

Figure 2. Diagram of continuous cord cooling system in this experimental setting. Circuit is composed of epidural cooling catheter, cooling unit, and circulating pump.

CSP

Spinal Cord Somatosensory Evoked Potentials

We recorded spinal cord somatosensory evoked potentials (sSEPs) directly from the spinal cord. Bipolar electrodes were positioned within the epidural space at the level of L3-L4 for stimulation and at the level of Th5-Th6 for recording. Stimulation parameters included a 0.2-ms pulse duration and a 3- to 5-mA current given at a rate of 5.0 Hz (Neuropack; Nihon Kohden Corporation, Tokyo, Japan). The sSEPs were recorded on a time base of 30 ms, passing through a bandpass filter of 50 to 1500 Hz. Each recording represented an average of 50 repetitions.

Neurologic Evaluation

Neurologic status with respect to hindlimb function was assessed at 12, 24, and 48 hours after surgery. A modified Tarlov score was used: 0 for complete paralysis, 1 for minimal movement, 2 for standing with assistance, 3 for standing alone but unable to walk, 4 for weak walking, and 5 for full recovery with normal walking.

Histologic Examination

After 48 hours, animals were deeply anesthetized and killed with an intravenous overdose of pentobarbital. The spinal cord was removed immediately and fixed in 10% formaldehyde solution for 2 weeks. For quantitative histopathologic analysis, the spinal cord was divided into five segments, consisting of the three lower thoracic and two lumbar segments. Representative sections of each segment of the spinal cord were stained with hematoxylin and eosin or fluorescent Nissl stain. Thirty-five specimens in each group were reviewed by an independent pathologist. Motor neurons (larger than 50 μm in diameter) with normal appearance were counted in each segment.

Statistical Analysis

We used the Mann–Whitney U test to compare postoperative neurologic status between groups of animals. Other parameters were compared between groups by analysis of variance for repeated measures or by the Student t test as appropriate.

Results

Baseline rectal temperature, spinal temperature, and epidural temperature were similar between groups A and B. In group A, baseline spinal temperature (35.1°C ± 0.8°C) and baseline epidural temperature at L4 level (35.2°C ± 0.8°C) had fallen significantly, to 26.5°C ± 2.4°C and 22.1°C ± 2.5°C, respectively, at the time of aortic crossclamping (P = .0001; Figure 3). At the conclusion of aortic crossclamping, spinal temperature and epidural temperature at L4 in group A had fallen further, to 25.4°C ± 2.2°C and 20.8°C ± 2.2°C, respectively. Rectal temperature in group A remained essentially constant. A significant difference was evident between spinal and rectal temperatures during aortic crossclamping in group A (P = .0001).

In group B, spinal, epidural, and rectal temperatures all remained constant throughout the procedure. Spinal temperature (35.3°C ± 0.6°C), epidural temperature at the levels of T5 (35.5°C ± 0.6°C) and L4 (35.3°C ± 0.6°C), and rectal temperature (36.2°C ± 0.4°C) at aortic crossclamping all did not differ significantly from one another within group B. No significant difference in rectal temperature between groups A and B was observed during the procedure (P = .64).

The mean aortic pressures during aortic crossclamping at the proximal aorta, the middle segment, and the distal aorta were similar between two groups (92.5 ± 13.8 mm Hg, 27.5 ± 5.2 mm Hg, and 8.7 ± 3.6 mm Hg, respectively, in group A, and 90.3 ± 15.9 mm Hg, 28.2 ± 4.7 mm Hg, and 9.6 ± 3.8 mm Hg, respectively, in group B, P = .50, P = .55, and P = .25, respectively).

Intrathecal Pressure

Intrathecal pressure was similar between groups during aortic crossclamping (group A 5.0 ± 1.6 mm Hg, group B 5.3 ± 1.6 mm Hg, P = .37). No significant elevation of intrathecal pressure was detected at aortic unclamping in group A (5.5 ± 1.2 mm Hg) relative to group B (5.8 ± 1.8 mm Hg; P = .94).

Spinal Cord Somatosensory Evoked Potentials

In group A, epidural cooling before aortic crossclamping significantly prolonged latency of sSEPs (2.47 ± 0.37 ms at baseline vs 3.24 ± 0.50 ms at aortic crossclamping, P = .01) and reduced their amplitude (35.5 ± 6.6 μV at baseline vs 12.5 ± 5.4 μV at aortic crossclamping, P = .0001). No

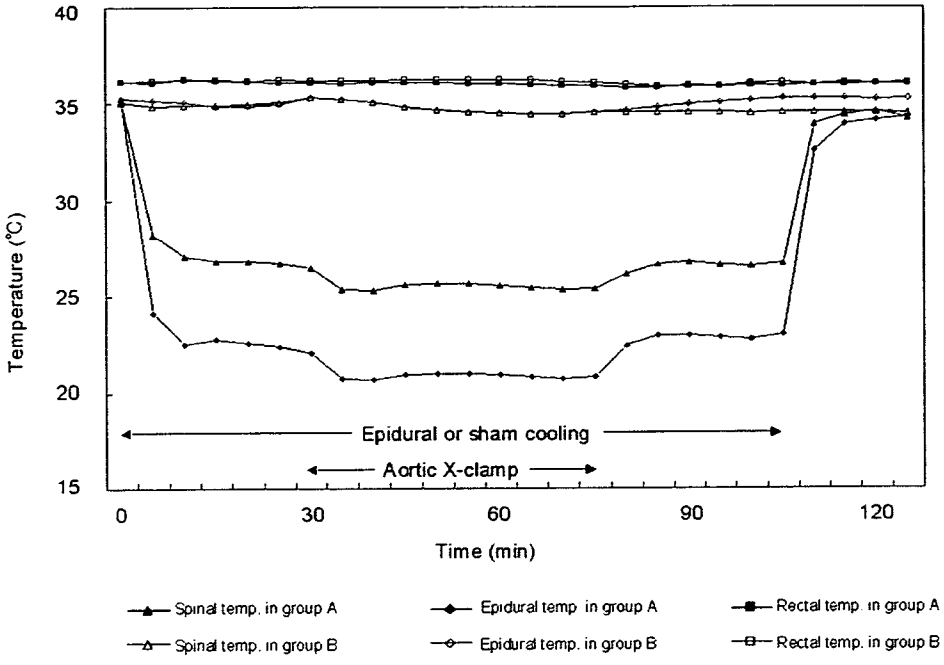

Figure 3. Changes in spinal, epidural (L4), and rectal temperatures during procedure. *Filled triangles, filled diamonds,* and *filled squares,* respectively, represent spinal, epidural, and rectal temperatures *(temp)* in cooling group (group A). *Open triangles, open diamonds,* and *open squares,* respectively, represent spinal, epidural, and rectal temperatures in control group (group B). *X-clamp,* Crossclamping.

pig showed abolition of sSEP waveforms as a result of epidural cooling itself.

Mean time from aortic crossclamping to onset of sSEP loss was significantly longer in group A than group B. Mean total time of sSEP loss and sSEP recovery time were significantly shorter in group A than in group B (Table 1).

The ratios of final amplitude of sSEPs to baseline amplitude (final amplitude/baseline) were 0.98 ± 0.12 in group A and 1.14 ± 0.31 in group B (P = .27). The ratios of final latency to baseline latency were 1.04 ± 0.03 in group A and 1.05 ± 0.04 in group B (P = .65).

Recovery of Motor Function

All 14 animals tolerated the period of aortic occlusion, survived the 48-hour recovery period after operation, and then underwent final neurologic evaluation. Group A animals showed significantly better neurologic scores at every point after operation than did group B (P = .001, Table 2).

TABLE 1. Loss and recovery of spinal cord somatosensory evoked potentials by group

			P value
Interval to potential loss (min)	28.4±6.6	18.3±5.0	.007
Total loss time (min)	19 ±6.7	31.3±5.9	.003
Recovery time (min)	2.4±1.1	4.6±1.8	.021

Data are expressed as mean ± SD.

Histologic Examination

Representative histologic sections from lumbar and thoracic segments of the cord are shown in Figure 4. In group A, motor neurons had a nearly normal appearance, with minimal eosinophilic change in the cytoplasm. Group B motor

TABLE 2. Neurologic outcome

Tarlov score	Cooling (n = 7)			Control (n = 7)		
	12 h	24 h	48 h	12 h	24 h	48 h
5	3	4	4	0	0	0
4	2	3	2	0	0	0
3	2	0	1	0	0	0
2	0	0	0	0	0	0
1	0	0	0	1	1	1
0	0	0	0	6	6	6

Hindlimb function in pigs was evaluated according to a modified Tarlov score at 12, 24, and 48 hr after surgery. Data represent numbers of animals with specified scores. Animals in epidural cooling group showed significantly better recovery than did those in control group (P = .001).